Hospital at Tokyo Medical and Dental University. These patients had synovial chondromatosis in the temporomandibular joint. Written informed consent was obtained from both the patients, and the experiments were approved by the hospital's Ethical Review Board.

BMP production by the synovium and free bodies in synovial chondromatosis. BMPs were detected by reverse transcription-polymerase chain reaction (RT-PCR) and immunohistochemistry. For the RT-PCR analysis, total RNA was extracted from unfixed frozen samples of the synovium and free bodies maintained at −80 °C and from cultured synovial cells by using NucleoSpin (Macherey-Nagel, Duren, Germany). RNA aliquots were reverse transcribed to complementary DNAs by using Oligo(dT) primer (Roche, Mannheim, Germany), deoxynucleotide triphosphate (dNTP; Promega), and Moloney murine leukemia virus (M-MuLV) reverse transcriptase (Fermentas, Hanover, MD). The complementary DNA products were subjected to PCR amplification, using gene-specific primers for *BMP-2, BMP-4, BMP-6,* and *BMP-7* (Table 1). The amplified products were electrophoresed on 2% agarose gel containing ethidium bromide, using OneSTEP ladder 100 (Nippon Gene, Japan).

For immunohistochemistry, synovium and a few enucleated free bodies were fixed in 10% phosphate-buffered formalin and embedded in paraffin. The free bodies were decalcified by treatment with 10% ethylenediaminetetraacetic acid (EDTA) at 4 °C for 1 week before embedding in paraffin. The embedded specimens were cut into 4 μm sections. Endogenous peroxidase activity was blocked with 10% hydrogen peroxidase/methanol, and nonspecific binding was blocked with 10% horse serum. Antigen retrieval was performed by incubating the specimens in an antigen retrieval buffer (10 mM Tris, 1 mM EDTA; pH 9.0) in a microwave at 80 °C for 60 min. The sections were incubated with goat anti-BMP-2/BMP-4 antibody (dilution, 1:500; Santa Cruz Biotechnology, Santa Cruz, CA), which specifically recognizes both BMP-2 and BMP-4. Anti-goat immunoglobulin G (IgG) (Vector laboratories, Burlingame, CA) was used as the secondary antibody. The antigen-bound peroxidase activity was visualized using 3,3'-diaminobenzidine chromogen.

Cell culture. To isolate cells from the free bodies and synovium obtained from our two patients, each tissue was cut into small pieces (approximately less than 1 × 1 mm), and the pieces were treated with 0.25% trypsin–EDTA solution at 37 °C for 20 min. After washing with phosphate-buffered saline (PBS) and Dulbecco's modified minimum essential medium (DMEM; Nacalai Tesque, Kyoto, Japan), the cells were re-incubated with DMEM containing 0.15% collagenase (Collagenase type II; Worthington Biochemical Corporation, Lakewood, NJ) and 0.25% trypsin (Becton, Dickinson and Company, Franklin Lakes, NJ) at 37 °C for 4 h. The harvested cells were inoculated into 24-well plates at a density of 2.0×10^4 cells per well and cultured in DMEM containing 10% fetal bovine serum (Invitrogen/Gibco, Carlsbad, CA), penicillin G (50 U/ml),

and streptomycin (50 mg/ml). The culture medium was changed every 3 days and maintained for 6 days with or without 500 ng/ml of recombinant human BMP-2 (rhBMP-2), which was provide by Astellas Pharma, Inc., Tokyo, Japan. To investigate the role of BMPs in chondrocyte and osteoblast differentiation, the cells isolated from the free bodies and synovium were cultured in the presence or absence of 500 ng/ml of noggin (R&D Systems, Minneapolis, MN).

RT-PCR analysis. Total RNA was extracted from the cultured cells and RNA aliquots were reverse transcribed to complementary DNAs as described above. The complementary DNA products were subjected to PCR amplification, using gene-specific primers for *Sox9, Col1a1, Col2a1, Col10a1, Aggrecan (Agc1), Runx2,* and *Osteocalcin* (Table 1). Real-time RT-PCR amplification was performed using a LightCycler System (Roche) with a Platinum SYBR Green qPCR SuperMix UDG kit (Invitrogen, Carlsbad, CA). The relative amount of each mRNA was normalized to β-actin mRNA.

Histochemical staining. Cultured cells were fixed in 10% phosphate-buffered formalin for 5 min, washed twice with 10 mM Tris–HCl (pH 7.5), and then double stained with alkaline phosphatase (ALP) and alcian blue. ALP staining was performed at 37 °C for 20 min by using 2-(4-iodophenyl)-3-(4-nitrophenyl)-5-phenyl-2H-tetrazolium chloride (INT) as a formazan dye with 5-bromo-4-chloro-3-indolyl phosphate (BCIP) as an enhancer (Roche). After the ALP staining, alcian blue (pH 2.5) staining was performed. Alcian blue-positive nodules were defined as those having a diameter of more than 50 μm.

Measurement of ALP activity. Cultured cells were sonicated in radioimmunoprecipitation assay (RIPA) buffer to obtain the cell lysate. ALP activity was determined using *p*-nitrophenylphosphate solution (Wako Pure Chemicals, Osaka, Japan) as the substrate. The amount of *p*-nitrophenylphosphate released was estimated by measuring the absorbance at 405 nm after 30 min of incubation at 37 °C. The protein concentration was determined using a bicinchoninic acid (BCA) protein assay kit (Thermo, Waltham, MA).

Statistical analyses. We used *t*-test for the statistical analysis of the influence of rhBMP-2 and noggin. *P* values less than 0.05 were considered significant. Each analysis was performed at least 3 times. The data are presented as mean ± standard error of mean (SEM) of independent replicates ($n \geqslant 3$).

Results and discussion

The synovium and free bodies expressed BMPs in synovial chondromatosis

In synovial chondromatosis, free bodies were produced in the joints (Fig. 1A), which are composed of cartilaginous tissues (Fig. 1B). We hypothesized that the synovium and free bodies synthesized BMPs, which might be involved in the excess formation of

Table 1
Primers sequences used for RT-PCR.

| Gene	Forward primer	Reverse primer
BMP-2	5'-GCAGTGCTACTGTTGAG	3'-AGATCAGCAATGTCTGGT
BMP-4	5'-AAGCGTAGCCCTAAGCATCA	3'-TGGTTGAGTTGAGGTGGTCA
BMP-6	5'-GCGACACCACAAAGAGTTCA	3'-CCCATACTACACGGGTGTCC
BMP-7	5'-GGTCATGAGCTTCGTCAACC	3'-GCAGGAAGAGATCCGATTCC
Sox9	5'-AGCAAAGGAGATGAAATCTGTTCTG	3'-AGAGTCTTGTGGTCGTCAATTGGA
Aggrecan	5'-AAGTATCATCAGTCCCAGAATCTAGCA	3'-TTGGTGGAGACGTAAGGTGC
Col1a1	5'-CACCAATCACCTGCGTACAGAA	3'-CAACACGCTACTGCACTAGACA
Col2a1	5'-CGAGTACCGATCACAGA	3'-ACTGCGGTTAGAAAGTATTTG
Col10a1	5'-GCCCGATCTTGTGTGC	3'-CTTACCTGCGTGCTGG
Runx2	5'-AGAAGGCACAGACAGAAGCTTGA	3'-TCACTAAATCCCGCGTAAGGA
Ocn	5'-GGCAGCGAGGTAGTCAAGAG	3'-CTGGAGAGGAGCAGAACTGG
β-Actin	5'-AAACTGGAACGGTGAAGGTG	3'-TCAAGTTGGGGGACAAAAAAG
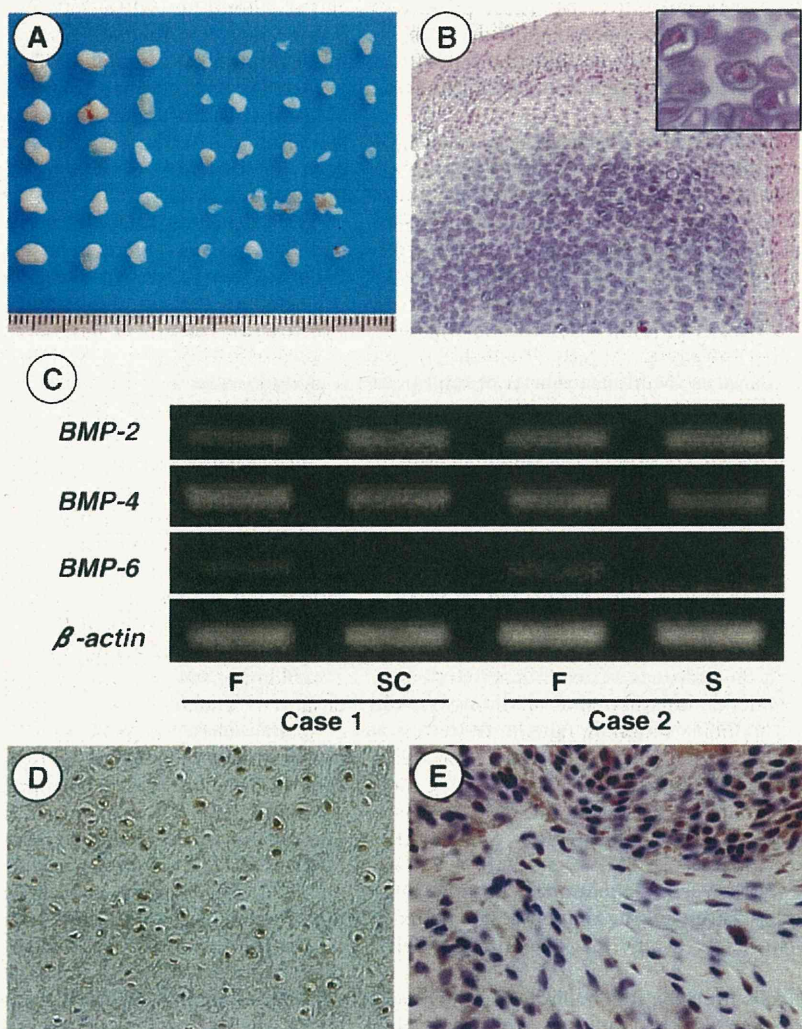
Fig. 1. Free bodies and BMP expression in synovial chondromatosis. (A) Gross findings of free bodies used for isolation of culture cells. Thirty-eight enucleated nodules were isolated from the temporomandibular joint in one patient. (B) Typical histology of a free body, which is composed of hyaline cartilage. Right upper insert shows a high magnification view of cartilage. (C) Expression of BMP-2, BMP-4, and BMP-6 mRNAs in the free bodies (F) and synovium (S) or cultured synovial cells (Sc). RT-PCR analysis was performed as described in Materials and methods. (D,E) Immunohistochemical detection of BMP-2/BMP-4 in the free bodies (D) and synovium (E). Immunoreactivity (brown) is seen in chondrocytes (D) and some fibroblastic cells (E). Immunohistochemistry was performed as described in Materials and methods.

cartilage or bone in synovial chondromatosis. To corroborate our hypothesis, we first investigated BMP expression in the synovium or cultured synovial cells and the free bodies isolated from two synovial chondromatosis patients. RT-PCR analysis revealed that the synovium or cultured synovial cells and the free bodies expressed high levels of BMP-2 and BMP-4 mRNAs (Fig. 1C). BMP-6 expression was weak in the free bodies and undetectable in the synovium or cultured synovial cells (Fig. 1C). No apparent BMP-7 expression was detected in either the synovium or the free bodies. Immunohistochemical study demonstrated that chondrocytes in the free bodies (Fig. 1D) and some fibroblastic cells in the synovium (Fig. 1E) expressed BMP-2/BMP-4. These results indicate the production of BMP-2 and BMP-4 by the free bodies and synovium in synovial chondromatosis and suggest the possible involvement of BMPs in the pathobiology of synovial chondromatosis. These results prompted us to further investigate the effects of rhBMP-2 on chondrogenic and osteogenic differentiation in the free-body and synovial cells isolated from synovial chondromatosis patients.

rhBMP-2 stimulated the production of cartilaginous nodules and ALP-positive cells in the culture of cells isolated from synovial chondromatosis patients

We first assessed the effects of rhBMP-2 on chondrogenic and osteogenic differentiation of cells by dual staining with ALP and alcian blue in the cells isolated from the free bodies and synovium. In the culture of free-body cells isolated from Case 1, we found numerous nodules composed of spherical cells associated with alcian blue-positive extracellular matrices, indicating chondrogenic differentiation (Fig. 2A). BMP-2 treatment (500 ng/ml) for 6 days increased the number of these nodules by 1.5 times than that in the BMP-2-untreated culture (Fig. 2B). Free-body cells isolated from Case 2 formed a few such nodules (Fig. 2B). Cultured synovial cells exhibited no apparent alcian blue-positive nodules in the presence or absence of BMP-2 (data not shown). These results indicate that free-body cells are capable of differentiating into chondrocytes more effectively than synovial cells.
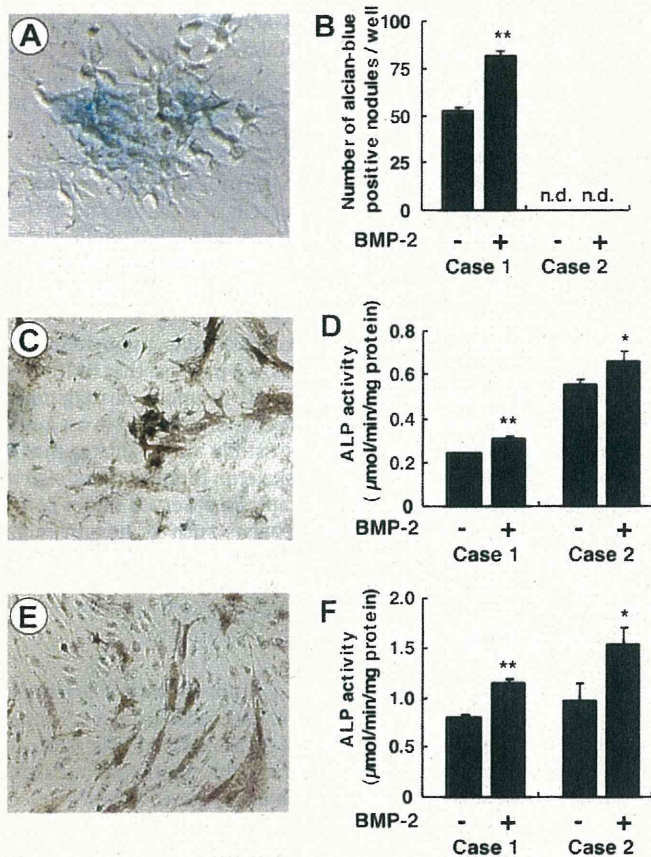
Fig. 2. Effects of rhBMP-2 on cartilaginous nodule formation (A,B) and ALP activity (C–F). (A) Double staining of the cultured cells isolated from the free bodies with ALP and alcian blue in the presence of rhBMP-2. Note that round-shaped alcian blue-positive cells (blue) form a cartilaginous colony. No ALP-positive cells are observed. (B) The number of alcian blue-positive colonies observed in culture of free-body cells and synovial cells in the presence or absence of rhBMP-2 (500 ng/ml). No positive colonies were observed in the synovial cell culture. (C,E) ALP histochemistry in free-body cells (C) and synovial cells (E). Numerous ALP-positive cells (brown) were observed in the cultures of free-body and synovial cells in the presence of rhBMP-2. (D,F) ALP activity in the free-body cells (D) and synovial cells (F) cultured with or without rhBMP-2.

ALP-positive cells were scattered in the cultures of both free-body (Fig. 2C) and synovial cells (Fig. 2E). Almost all the cells were polyhedral or spindle-shaped without any close association with the alcian blue-positive nodules (Fig. 2C and E). BMP-2 treatment increased the number of ALP-positive cells in the cultures of both the free-body and synovial cells (data not shown). Further, BMP-2 treatment significantly increased ALP activity in both the free-body cells (Fig. 2D) and the synovial cells (Fig. 2F). ALP activity is exhibited from early differentiated osteoblasts through mature osteoblasts [8], but it appears in only mature hypertrophic cells during chondrocyte differentiation. We found few nodules double-positive for ALP and alcian blue even in the cultures treated with rhBMP-2. These suggest that ALP-positive polyhedral or spindle-shaped cells are osteoblast lineage cells.

BMP-2 stimulated the expression of mRNAs related to chondrocyte and osteoblast differentiation in the culture of cells isolated from synovial chondromatosis patients

We investigated the effects of rhBMP-2 on the expression of mRNAs related to chondrocyte differentiation. The basal expres-

sion levels of *Sox9*, *Col2a1*, *Aggrecan*, and *Col10a1* mRNAs were significantly higher in the free-body cells than in the synovial cells (data not shown). BMP-2 treatment increased *Sox9* mRNA expression over 20-fold in the free-body cells (Fig. 3A). BMP-2 also significantly increased the expression of *Col12a1* and *Aggrecan* mRNAs, which are involved in the early differentiation of chondrocytes [22] (Fig. 3A). The expression of *Col10a1* mRNA, which is mainly expressed by hypertrophic chondrocytes [22], was also stimulated by the BMP-2 treatment, but its induction in the treated culture was less than 2-fold as compared with that in the control cultures (Fig. 3A). In the synovial cells, rhBMP-2 treatment significantly increased the expression of *Sox9*, *Col2a1*, and *Aggrecan* mRNAs (Fig. 3B). BMP-2 increased *Col10a1* expression more effectively in the synovial cells than in the free-body cells. These results indicate that rhBMP-2 stimulates the free-body and synovial cells to differentiate into chondrogenic cells.

We next investigated the effects of rhBMP-2 on the expression of mRNAs related to osteoblast differentiation. BMP-2 treatment significantly increased *Runx2* expression but failed to stimulate *Col1a1* expression in the free-body cells. rhBMP-2 slightly, but significantly, increased *Osteocalcin* expression in only Case 2. In the synovial cells, BMP-2 treatment significantly increased the expression of *Runx2*, *Col1a1*, and *Osteocalcin* mRNAs. These results suggest that rhBMP-2 induces osteoblast differentiation more effectively in synovial cells than in free-body cells.

Taken together, these results indicate that BMP-2 treatment stimulates chondrocyte and osteoblast differentiation in free-body and synovial cells. Our histopathological examination of eight patients with synovial chondromatosis in the temporomandibular joint revealed that free bodies in all the cases exhibited extensive cartilage formation, and only one case was associated with bone formation (unpublished results). These findings support that the
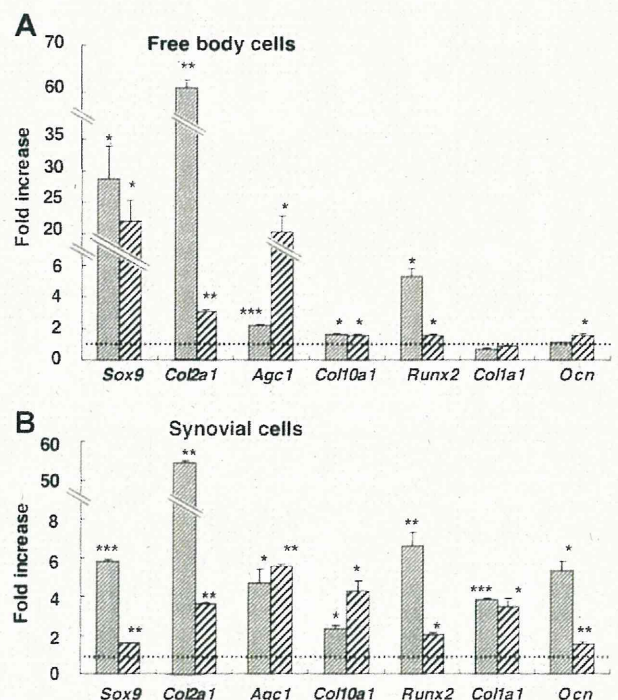

Fig. 3. Effects of BMP-2 on the expression of mRNAs related to chondrocyte and osteoblast differentiation in the free-body cells (A) and synovial cells (B). The cells were cultured for 6 days in the presence or absence of BMP-2 (500 ng/ml), and the expression of mRNAs was determined by real-time RT-PCR analysis as described in Materials and methods. Agc1, Aggrecan. Thin slash bars indicate the data of Case 1, and thick slash bars show that of Case 2. $^*P < 0.05$, $^{**}P < 0.01$, $^{***}P < 0.001$ ($n = 3$).

free-body cells used in the present study had differentiated into chondrogenic cells, and the synovial cells retained bipotency to differentiate into both chondrocytes and osteoblasts.

Noggin inhibited the expression of marker genes related to chondrocyte and osteoblast differentiation in the cultured cells

The free-body and synovial cells expressed substantial levels of mRNAs related to chondrocyte and osteoblast differentiation in the absence of exogenous BMP-2. We also demonstrated that the free-body and synovial cells expressed BMPs. These results suggested that endogenous BMPs synthesized by the free-body and synovial cells stimulated chondrocyte and osteoblast differentiation in an autocrine or a paracrine fashion. To address this issue, we investigated the effects of noggin, which is a specific antagonist for BMPs [23,24], on chondrogenic and osteoblastic differentiation in the free-body and synovial cells.

Noggin significantly inhibited *Sox9* and *Col2a1* expression in both the free-body and synovial cells (Fig. 4A and B). Noggin also inhibited aggrecan expression in the free-body cells but not in the synovial cells (Fig. 4A and B), which might be due to the low level of basal aggrecan mRNA expression in the latter. The inhibitory effect of noggin on *Col10a1* expression was observed in only one case each in the free-body and synovial cells (Fig. 4A and B). These results indicate that BMPs synthesized by free-body and synovial cells are involved in chondrogenic differentiation in synovial chondromatosis.

Noggin significantly inhibited *Runx2* expression in the free-body and synovial cells, but its inhibitory effect on *Col1a1* expression was observed in only synovial cells isolated from Case 1 (Fig. 4A and B). Noggin inhibited *Osteocalcin* expression in the synovial cells but not in the free-body cells (Fig. 4A and B). The ALP activity in the free-body (Fig. 4C) and synovial cells (Fig. 4D) was also inhibited by noggin. These results suggest that BMPs synthesized by free-body and synovial cells also participate in the regulation of osteoblast differentiation in synovial chondromatosis.

In conclusion, the present study demonstrated that the free bodies and synovium isolated from synovial chondromatosis patients produced BMPs and that the free-body and synovial cells are capable of differentiating into chondrocyte and osteoblast lineage cells in response to BMPs. Thus, we propose that BMPs synthesized by synovial and free-body cells promote cartilaginous and osteogenic metaplasia in synovial chondromatosis in an autocrine or a paracrine fashion. The present study also indicates that BMPs play important roles in not only skeleton formation but also in the cartilaginous and osteogenic metaplasia observed under pathological conditions. Thus, BMP antagonists such as noggin might be useful therapeutic tools for preventing chondrogenic metaplasia occurred in synovial chondromatosis.

Acknowledgments

References

[1] F.P. Murphy, D.C. Dahlin, C.R. Sullivan, Articular synovial chondromatosis, J. Bone Joint Surg. Am. 44 (1962) 77–86.
[2] V. Karlis, R.S. Grickman, M. Zaslow, Synovial chondromatosis of the temporomandibular joint with intracranial extension, Oral Surg. Oral Med. Oral Pathol. Oral Radiol. Endod. 86 (1998) 664–666.
[3] J.J. von Lindern, I. Theuerkauf, B. Niederhagen, S. Bergé, T. Appel, R.H. Reich, Synovial chondromatosis of the temporomandibular joint: clinical, diagnostic, and histomorphologic findings, Oral Surg. Oral Med. Oral Pathol. Oral Radiol. Endod. 94 (2002) 31–38.
[4] F. Mertens, K. Jonsson, H. Willén, A. Rydholm, A. Kreicbergs, L. Eriksson, G. Olsson-Sandin, F. Mitelman, N. Mandahl, Chromosome rearrangements in synovial chondromatous lesions, Br. J. Cancer 74 (1996) 251–254.
[5] R. Sciot, P. Dal Cin, J. Bellemans, I. Samson, H. Van den Berghe, V.B. Damme, Synovial chondromatosis: clonal chromosome changes provide further evidence for a neoplastic disorder, Virchows Arch. 433 (1998) 189–191.
[6] B.L. Sperling, S. Angel, G. Stoneham, V. Chow, A. McFadden, R. Chibbar, Synovial chondromatosis and chondrosarcoma: a diagnostic dilemma, Sarcoma 7 (2003) 69–73.
[7] R.L. Davis, H. Foster, K. Arthur, S. Trewin, P.W. Hamilton, D.J. Biggart, Cell proliferation studies in primary synovial chondromatosis, J. Pathol. 184 (1998) 18–23.
[8] A. Yamaguchi, T. Komori, T. Suda, Regulation of osteoblast differentiation mediated by bone morphogenetic proteins, hedgehogs, and Cbfa1, Endocr. Rev. 21 (2000) 393–411.
[9] G.A. Rodan, S. Harada, The missing bone, Cell 30 (1997) 677–680.
[10] E.J. Jin, S.Y. Lee, Y.A. Choi, J.C. Jung, O.S. Bang, S.S. Kang, BMP-2-enhanced chondrogenesis involves p38 MAPK-mediated down-regulation of Wnt-7a pathway, Mol. Cells 22 (2006) 353–359.
[11] W. Bi, J. Min Deng, Z. Zhang, R. Behringer, B. de Crombrugghe, Sox9 is required for cartilage formation, Nat. Genet. 22 (1999) 85–89.
[12] Y. Mori-Akiyama, H. Akiyama, D.H. Rowitch, B. de Crombrugghe, Sox9 is required for determination of the chondrogenic cell lineage in the cranial neural crest, Proc. Natl. Acad. Sci. USA 100 (2003) 9360–9365.
[13] P. Ducy, R. Zhang, V. Geoffroy, A.L. Ridall, G. Karsenty, Osf2/Cbfa1: a transcriptional activator of osteoblast differentiation, Cell 89 (1997) 747–754.
[14] T. Komori, H. Yagi, S. Nomura, A. Yamaguchi, K. Sasaki, K. Deguchi, Y. Shimizu, R.T. Bronson, Y.-H. Gao, M. Inada, M. Sato, R. Okamoto, Y. Kitamura, S. Yoshiki, T. Kishimoto, Targeted disruption of Cbfa1 results in a complete lack of bone formation owing to maturational arrest of osteoblasts, Cell 89 (1997) 755–764.
[15] K. Katagiri, A. Yamaguchi, K. Komaki, E. Abe, N. Takahashi, T. Ikeda, V. Rosen, J.M. Wozney, A. Fujisawa-Sehara, T. Suda, Bone morphogenetic protein-2 converts the differentiation pathway of C2C12 myoblasts into the osteoblast lineage, J. Cell. Biol. 127 (1994) 1755–1766.
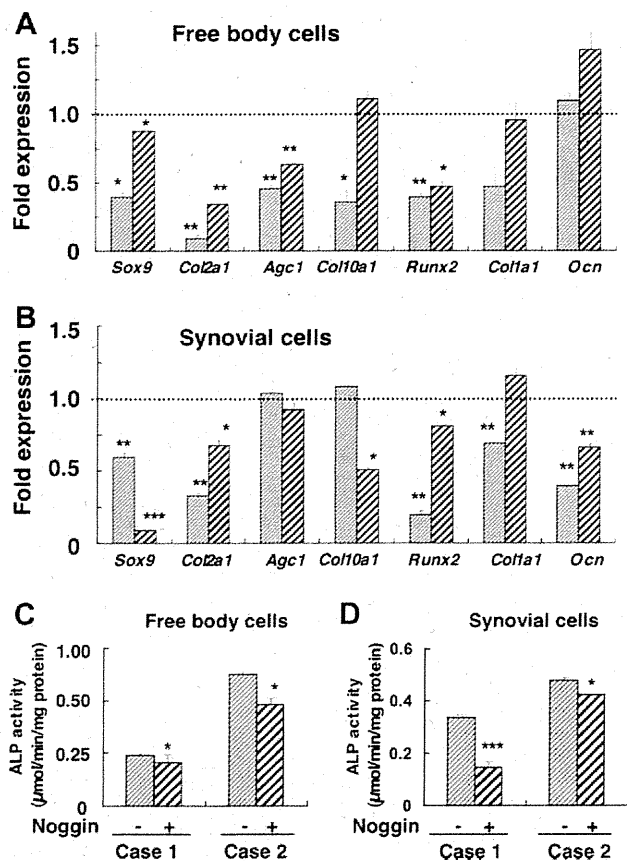

Fig. 4. Effects of noggin on the expression of mRNAs related to chondrocyte and osteoblast differentiation in the free-body cells (A) and synovial cells (B). The cells were cultured for 6 days in the presence or absence of noggin (500 ng/ml), and the expression of mRNAs was determined by real-time RT-PCR analysis as described in Materials and methods. Agc1, Aggrecan. Thin slash bars indicate the data of Case 1, and Thick slash bars show that of Case 2. $^*P < 0.05$, $^{**}P < 0.01$, $^{***}P < 0.001$ ($n = 3$).

[16] R.J. Lories, I. Derese, J.L. Ceuppens, F.P. Luyten, Bone morphogenetic proteins 2 and 6, expressed in arthritic synovium, are regulated by proinflammatory cytokines and differentially modulate fibroblast-like synoviocyte apoptosis, Arthritis Rheum. 48 (2003) 2807–2818.

[17] R.J.U. Lories, F.P. Luyten, Bone morphogenetic protein signaling in joint homeostasis and disease, Cytokine Growth Factor Rev. 16 (2005) 287–298.

[18] K. Bobacz, I.G. Sunk, S. Hayer, L. Amoyo, M. Tohidast-Akrad, G. Kollias, J.S. Smolen, G. Schett, Differentially regulated expression of growth differentiation factor 5 and bone morphogenetic protein 7 in articular cartilage and synovium in murine chronic arthritis: potential importance for cartilage breakdown and synovial hypertrophy, Arthritis Rheum. 58 (2008) 109–118.

[19] H. Iwata, S. Ono, K. Sato, T. Sato, M. Kawamura, Bone morphogenetic protein-induced muscle- and synovium-derived cartilage differentiation in vitro, Clin. Orthop. Relat. Res. 296 (1993) 295–300.

[20] N. Shintani, E.B. Hunziker, Chondrogenic differentiation of bovine synovium: bone morphogenetic proteins 2 and 7 and transforming growth factor beta1 induce the formation of different types of cartilaginous tissue, Arthritis Rheum. 56 (2007) 1869–1879.

[21] S. Yamane, A.H. Reddi, Induction of chondrogenesis and superficial zone protein accumulation in synovial side population cells by BMP-7 and TGF-beta1, J. Orthop. Res. 26 (2008) 485–492.

[22] M.B. Goldring, K. Tsuchimochi, K. Ijiri, The control of chondrogenesis, J. Cell. Biochem. 97 (2006) 33–44.

[23] V. Rosen, BMP and BMP inhibitors in bone, Ann. N. Y. Acad. Sci. 1068 (2006) 19–25.

[24] L.J. Brunet, J.A. McMahon, A.P. McMahon, R.M. Harland, Noggin, cartilage morphogenesis, and joint formation in the mammalian skeleton, Science 280 (1998) 1455–1457.

Deficiency of Chemokine Receptor CCR1 Causes Osteopenia Due to Impaired Functions of Osteoclasts and Osteoblasts*[S]

Akiyoshi Hoshino,[a,b,c1] Tadahiro Iimura,[d2,3] Satoshi Ueha,[e] Sanshiro Hanada,[a] Yutaka Maruoka,[a,f4]
Mitsuori Mayahara,[g] Keiko Suzuki,[h] Toshio Imai,[i] Masako Ito,[j] Yoshinobu Manome,[c] Masato Yasuhara,[b]
Takaaki Kirino,[k] Akira Yamaguchi,[d2] Kouji Matsushima,[e5] and Kenji Yamamoto[a,b6]

From the [a]International Clinical Research Center, Research Institute, International Medical Center of Japan, Tokyo 162-8655, the
[e]Department of Molecular Preventive Medicine, Graduate School of Medicine, The University of Tokyo, Tokyo 113-0033, the
Departments of [b]Pharmacokinetics and Pharmacodynamics (Hospital Pharmacy) and [d]Oral Pathology, Global Center of
Excellence, Tokyo Medical and Dental University, Tokyo 113-8519, the [c]Department of Molecular Cell Biology, Institute of DNA
Medicine, Research Center for Medical Sciences, Jikei University School of Medicine, Tokyo 105-8461, the [f]Department of Dentistry
and Oral Surgery, Toyama National Hospital, International Medical Center of Japan, Tokyo 162-8655, the Departments of [g]Oral
Histology and [h]Pharmacology, Showa University School of Dentistry, Tokyo 142-8555, the [i]Kan Research Institute, Inc.,
Kobe 650-0047, the [j]Department of Radiology, Nagasaki University School of Medicine, Nagasaki 852-8501, and the [k]International
Medical Center of Japan, Tokyo 162-8655, Japan

Chemokines are characterized by the homing activity of leukocytes to targeted inflammation sites. Recent research indicates that chemokines play more divergent roles in various phases of pathogenesis as well as immune reactions. The chemokine receptor, CCR1, and its ligands are thought to be involved in inflammatory bone destruction, but their physiological roles in the bone metabolism *in vivo* have not yet been elucidated. In the present study, we investigated the roles of CCR1 in bone metabolism using CCR1-deficient mice. $Ccr1^{-/-}$ mice have fewer and thinner trabecular bones and low mineral bone density in cancellous bones. The lack of CCR1 affects the differentiation and function of osteoblasts. *Runx2*, *Atf4*, *Osteopontin*, and *Osteonectin* were significantly up-regulated in $Ccr1^{-/-}$ mice despite sustained expression of *Osterix* and reduced expression of *Osteocalcin*, suggesting a lower potential for differentiation into mature osteoblasts. In addition, mineralized nodule formation was markedly disrupted in cultured osteoblastic cells isolated from $Ccr1^{-/-}$ mice. Osteoclastogenesis induced from cultured $Ccr1^{-/-}$ bone marrow cells yielded fewer and smaller osteoclasts due to the abrogated cell-fusion. $Ccr1^{-/-}$ osteoclasts exerted no osteolytic activity concomitant with reduced expressions of *Rank* and its downstream targets, implying that the defective osteoclastogenesis is involved in the bone phenotype in $Ccr1^{-/-}$ mice. The co-culture of wild-type osteoclast precursors with $Ccr1^{-/-}$ osteoblasts failed to facilitate osteoclastogenesis. This finding is most likely due to a reduction in *Rankl* expression. These observations suggest that the axis of CCR1 and its ligands are likely to be involved in cross-talk between osteoclasts and osteoblasts by modulating the RANK-RANKL-mediated interaction.

Chemokines are initially identified as small cytokines that direct the homing of circulating leukocytes into sites of inflammation (1). Chemokines are now recognized to be major factors in inflammation and immune development as well as tumor growth, angiogenesis, and osteolysis. Chemokine receptors are expressed in a well organized spatiotemporal manner in various types of leukocytes, including lymphocytes, granulocytes, and macrophages. They facilitate the recruitment of these cells into inflammatory sites during the appropriate phase of inflammation.

Recent findings indicate that chemokine receptors, including CCR1[7] and its related chemokines, CCL3 and CCL9, are involved in the pathogenesis of a variety of diseases. In particular, CCL3 (also called MIP-1α), a major pro-inflammatory chemokine produced at inflammatory sites, appears to play a crucial role in pathological osteoclastogenesis (2, 3). In osteolytic bone inflammation (*e.g.* rheumatoid arthritis-associated bone destruction), CCL3 induces ectopic osteoclastogenesis (4)

---

and results in bone destruction (5). Several reports suggested that CCL3 is also produced by myeloma cells and directly stimulates bone destruction in myeloma-related bone diseases (5–7). These findings indicate the possible roles of CCL3 as a crucial chemokine for osteoclast function. Several antagonists of the chemokine ligands of CCL3, such as CCR1-specific (BX471) and CCR5-specific (TAK779) blockers, have been tested as drug candidates for the treatment of patients with rheumatoid arthritis-associated bone destruction and multiple myeloma (4, 8). The chemokine CCL9 (also called MIP-1γ), is also abundantly produced by various myeloid lineage-derived cells, including osteoclasts (9), activates osteoclastogenesis through its receptor, CCR1 (10–12). However, the exact physiological functions of CCR1 and its related chemokines in bone remodeling are still not fully characterized (12, 13).

A recent study using an ovariectomy-induced bone loss model found that the chemokine receptor CCR2 was associated with postmenopausal bone loss (14), but there are few reports on bone phenotypes in other chemokine receptor-deficient mouse models. In the present study, we demonstrated that osteopenia in $Ccr1^{-/-}$ mice appeared to be due to impaired osteoclast and osteoblast function. Our data also uncovered a possible role for CCR1 and its related ligands in the communication between osteoclasts and osteoblasts.

EXPERIMENTAL PROCEDURES

Mice—Standard male C57BL/6 mice (6–9 weeks of age) were obtained from CLEA Japan. $Ccr1^{-/-}$ mice (15) purchased from Jackson Laboratories were backcrossed for 8–10 generations on the C57BL/6 background mice. Mice were all bred and maintained under pathogen-free conditions at the animal facilities of the University of Tokyo. All experiments were performed according to the Institutional Guidelines for the Care and Use of Laboratory Animals in Research and were approved by the ethics committees of both the University of Tokyo and the Research Institute of International Medical Center of Japan.

Materials—Recombinant mouse M-CSF and RANKL were purchased from R&D Systems Inc. (Minneapolis, MN) and PeproTech Inc. (Rocky Hill, NJ), respectively. Recombinant mouse CCL2 (MCP-1), CCL3 (MIP-1α), CCL4 (MIP-1β), CCL5 (RANTES), CCL9 (MIP-1γ), and CCL11 (eotaxin-1) and their corresponding-neutralizing antibodies were purchased from R&D Systems. Control rat IgG was purchased from Jackson ImmunoResearch (Bar Harbor, ME). Recombinant mouse CX3CL1 (fractalkine) was purchased from R&D Systems. Hamster anti-CX3CL1-neutralizing antibody and control hamster IgG were kindly provided by Dr. Toshio Imai (Kan Research Institute, Kobe, Japan). Rabbit anti-human/mouse CCR1 polyclonal antibody and control rabbit IgG were purchased from AbCam (Cambridge, MA) and Chemicon (Temecula, CA), respectively. Secondary antibodies (Alexa488-labeled anti-rabbit IgG and Streptavidin-PE) were purchased from Molecular Probes (Eugene, OR). Rabbit anti-TRAP and anti-Cathepsin K polyclonal antibodies were both purchased from Santa Cruz Biotechnology (Santa Cruz, CA).

Osteoclast and Osteoblastic Cell Culture—Mouse bone marrow cells cultured in α-minimal essential medium were used as sources of osteoclastic and osteoblastic cell cultures. The non-adherent cells were collected for bone marrow-derived macrophage and pre-osteoclast induction, and adherent bone marrow-derived mesenchymal stromal cells were collected for osteoblast induction. Bone marrow-derived macrophages were induced with 10 ng/ml M-CSF for an additional 10 days. To generate pre-osteoclasts, non-adherent cells were passed through a column filled with Sephadex G-10 microspheres (Amersham Biosciences) and were then cultured with 10 ng/ml M-CSF and 20 ng/ml RANKL for 4 days. The mature osteoclasts were induced from pre-osteoclasts by culturing for an additional 14 days with M-CSF and RANKL. The culture media were replaced every 3 days. TRAP activity in the osteoclasts was determined by staining using an acid phosphatase leukocyte staining kit (Sigma). The contamination of stromal/osteoblastic cells was monitored using Q-PCR analysis, as a low expression level of the *Osteoprotegrin* gene indicates stromal/osteoblastic cells.

Osteoblastic differentiation in adherent bone marrow mesenchymal stromal cells was induced by culture in α-minimal essential medium containing 10% FBS, 200 μM ascorbic acid, 10 mM β-glycerophosphate, and 10 nM dexamethasone (16). The culture media was replaced once every 3 days in the presence or absence of chemokine-neutralizing antibodies. The cells were fixed with 4% paraformaldehyde and stained for alkaline phosphatase with naphthol AS-MX phosphate plus Fastblue-BB (Sigma) and for minerals with alizarin red. Mineral deposition was alternatively identified by von Kossa staining (Polysciences, Inc., Warrington, PA), and the mineralized areas were measured by using an Array Scan VTI HCS analyzer (Beckman Coulter).

Co-culture experiments with osteoclast precursors and osteoblasts were performed by inoculating bone marrow-derived precursors (1×10^5 cells/well) onto the layer of osteoblastic cells that had been cultured for 21 days with osteoblast-inducing media in 24-well plates. Thereafter, these cells were co-cultured for 7 days in α-minimal essential medium supplemented with 10% FBS and 10 μg/ml vitamin D_3. To assess bone resorption activity, these co-culture studies were also conducted using bone slices. After fixation of the cells with 2.5% glutaraldehyde/1.6% paraformaldehyde in 0.1 M cacodylic acid (pH 7.4), the bone slices were briefly rinsed, and were completely dehydrated in an ascending series of ethanol and liquid carbon dioxide. The samples were coated with an ultrafine titanium oxide powder and observed under a scanning electron microscopy.

Immunohistochemical Staining—For the immunohistochemical staining analyses, osteoclasts were fixed with 4% paraformaldehyde, permeabilized, and stained with the indicated specific antibodies, followed by Alexa594-conjugated secondary antibodies and Alexa488-labeled phalloidin (Molecular Probes). The osteoclasts with multiple nuclei (>3) were quantified. Images were captured using an IX-81 fluorescence microscope equipped with a confocal microscopy DSU unit (Olympus, Japan) and were analyzed with the MetaMorph™ software program (Universal Imaging, Molecular Devices, Sunnyvale, CA). The formation of osteoclasts was quantified by capturing and analyzing images using the ImageJ software program (National Institutes of Health, Bethesda, MD) based on

TRAP staining of 25 fields in each well, which were randomly chosen and analyzed.

Real-time PCR Analysis—Total cellular RNA from osteoclasts, osteoblasts, and bone tissues (proximal tibia after the bone marrow flush and the removal of metaphysial regions) was isolated using the RNeasy kit (Qiagen, Valencia, CA). The total RNA was then reverse-transcribed into cDNA using the Superscript III RT kit (Invitrogen). The real-time quantitative PCR analyses were performed using the ABI 7700 sequence detector system with SYBR Green (Applied Biosystems, Foster City, CA). The sequences were amplified for 40 cycles under the following conditions: denaturation at 95 °C for 15 s, annealing at 60 °C for 30 s, and extension at 72 °C for 45 s with primers for the chemokine receptors as previously reported (17). Gene expression levels were compared with *Gapdh* gene expression by the $2^{-\Delta(Ct)}$ method.

Measurement of Cytokines and Chemokines—Chemokine CCL5 and CCL9 secretion levels were determined by ELISA using the antibodies MAB4781 and BAF478 (R&D systems) and MAB463 and BAF463 (R&D systems), respectively. The reaction intensities were determined by using HRP-conjugated streptavidin (Chemicon). The cytokine production levels were quantified with a mouse 23-plex multiple cytokine detection system (Bio-Rad Corp., Hercules, CA) according to the manufacturer's instructions.

Flow Cytometry—FITC-, PE-, APC-, PerCP-Cy5.5-, PE-Cy7-, or biotin-conjugated anti-mouse mAbs to CD45.2 (104), CD115 (AFS98), and CD265/RANK (R12–31), and subclass-matched control antibodies were purchased from eBioscience (San Diego, CA). Anti-mouse mAbs to FcγR (2.4G2), Ly6C/6G (RB6–8C5), CD11b (M1/70), and CD19 (1D3) were purchased from BD Pharmingen (San Diego, CA). The flow cytometric analyses were performed using an LSR II flow cytometer with the FACS diva software program (BD Biosciences) and were analyzed with the FlowJo software program (TreeStar, Ashland, OR). Dead cells were excluded on the basis of the forward and side scatter profiles and propidium iodide staining.

Microcomputed Tomography and Peripheral Quantitative Computed Tomography—Micro-computed tomography (microCT) scanning was performed on proximal tibiae by μCT-40 (SCANCO Medical AG) with a resolution of 12 μm, and the microstructure parameters were three-dimensionally calculated as previously described (18). The bone scores were measured by peripheral quantitative CT using the XCT Research SA+ system (Stratec Medizintechnik GmbH, Pforzheim, Germany). The bone scores and density were measured and analyzed at 1.2 mm below the epiphyseal plate of distal femora. The scores were defined according to the American Society for Bone and Mineral Research standards.

Bone Histomorphometry—The unilateral proximal tibiae fixed with ethanol were embedded in glycol methacrylate, and the blocks were cut in 5-μm-thick sections. The structural parameters were analyzed at the secondary spongiosa. For the assessment of dynamic histomorphometric indices, calcein (at a dose of 20 mg/kg body weight) was injected twice (72-h interval) to wild-type and *Ccr1*-deficient mice, respectively. The sections were stained with toluidine blue and analyzed using a semi-automated system (Osteoplan II, Zeiss). The nomencla-

ture, symbols, and units used in the present study are those recommended by the Nomenclature Committee of the American Society for Bone and Mineral Research (19).

Measurement of TRAP, BALP, and Collagen-type I N-telopeptides (NTx)—Tartrate-resistant acid phosphatases (TRAP5b) in serum and culture supernatant were measured by the mouse TRAP EIA assay kit (Immunodiagnostic system, Fountain Hills, AZ). In brief, the culture supernatant or diluted serum was applied to an anti-TRAP5b-coated microplate, according to the manufacturer's instruction. The enzymatic activities of bound TRAP were determined with chromogenic substrates. Bone-specific alkaline phosphatase (BALP) levels were measured using the mouse BALP ELISA kit (Cusabio Biotech Co. Ltd., Wilmington, DE). Collagen-type I NTx were measured by ELISA (SRL, Tokyo).

Collagen-based Zymography—Collagen digestion activity was measured by using modified methods, which were based on gelatin-based zymography (20), with some modification for type-I collagen (21, 22). In brief, the osteoclasts were gently digested with lysis buffer (150 mM NaCl, 50 mM HEPES, 5 mM EDTA, and 10% Nonidet P-40 with Halt protease inhibitor mixture, pH 7.5). The lysates were separated by SDS-PAGE on a 10% polyacrylamide gel with porcine type-I collagen (1 mg/ml, Nitta Gelatin Inc., Osaka, Japan) under chilled conditions. The gel was washed with denaturation buffer (Tris-buffered saline (150 mM NaCl, 25 mM Tris-HCl, pH 7.4, supplemented with 2.5% Triton X-100) and then subjected to zymography for 18–24 h at 37 °C in zymography developing buffer (Tris-buffered saline, supplemented with 1 mM CaCl$_2$, 1 μM ZnCl$_2$, and 0.05% Brij-35). The signals were detected using Coomassie Brilliant Blue solution (Wako Pure Chemicals, Osaka, Japan).

Immunoblot Analysis—Total cell lysates were isolated, separated by SDS-PAGE, and electrotransferred onto Immobilon-P PVDF membranes (Millipore). The membrane was blocked by 5% BSA in TBST (150 mM NaCl, 25 mM Tris-HCl (pH 7.4) supplemented with 0.1% Tween 20) and incubated with rabbit anti-ATF4 polyclonal antibody (1/2,000), followed by HRP-conjugated anti-rabbit IgG (1/10,000). The signals were detected using an ECL chemiluminescence substrate (Amersham Biosciences). The quantitative analysis of blots was normalized using the lumino image analyzer LAS-4000 (Fujifilm Corp., Japan).

Statistics—Data are presented as the mean ± S.E. for the indicated number of independent experiments. Statistical significance was determined with a post-hoc test of one-factor factorial analysis of variance (Figs. 3E, 6D, 7B, and 7C), the Wilcoxon Mann-Whitney U test (non-parametric analysis, Fig. 2C, and Fig. 6C), and Student's t test (other figures) using the KaleidaGraph® 4.0 programs (Synergy Software, Reading, PA). Differences with a p value of <0.05 was considered statistically significant (* and # indicate up-regulation and down-regulation, respectively; NS indicates not significant).

RESULTS

CCR1-deficient Mice Exhibit Osteopenia—To understand the functions of CCR1 in bone metabolism, we investigated the bone mineral density in $Ccr1^{-/-}$ mice. A peripheral quantitative CT analysis showed a significant reduction in bone mineral
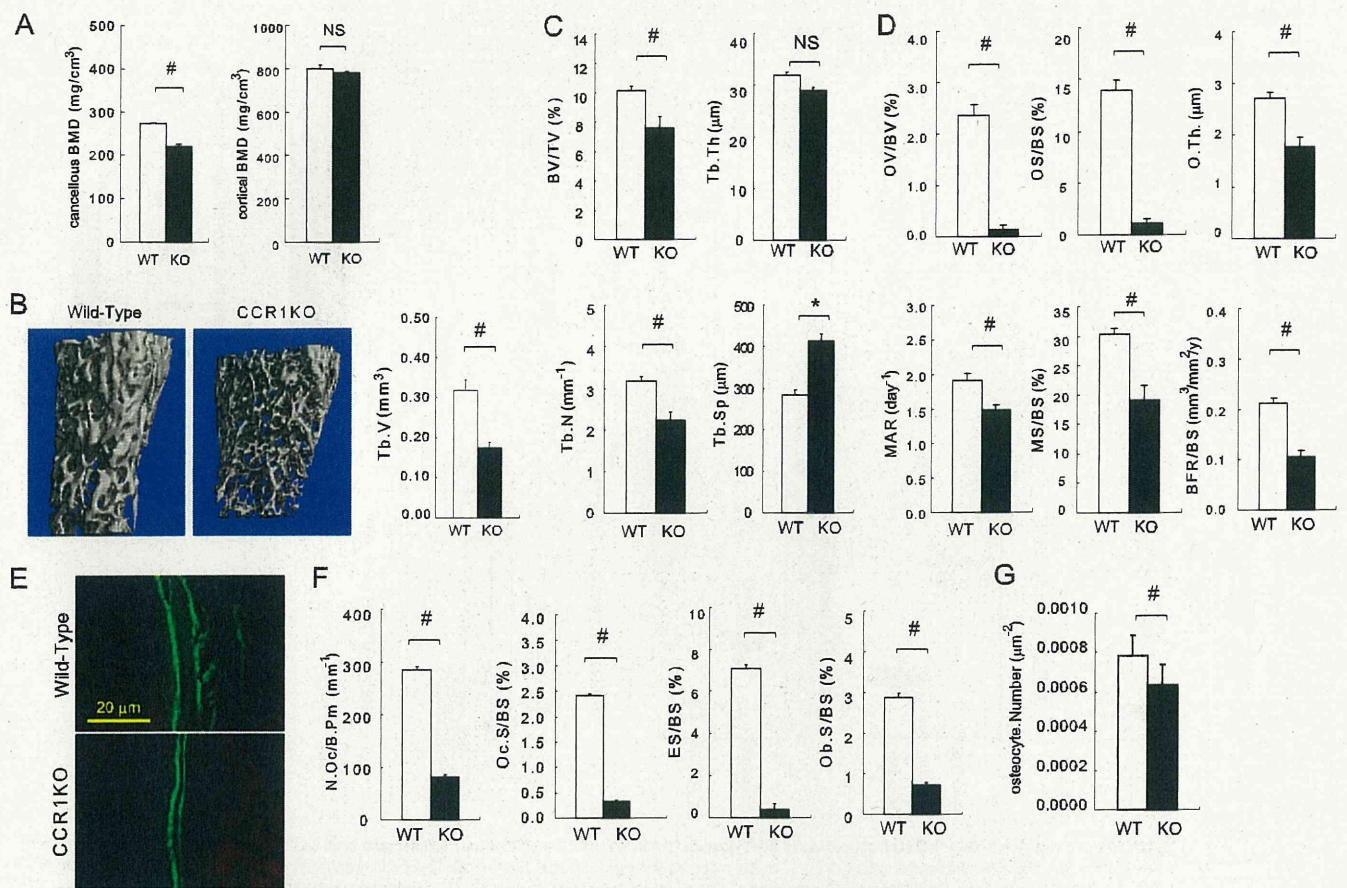
FIGURE 1. **Bone morphometric analyses of CCR1$^{-/-}$ mice.** *A* shows the bone mineral density of trabecular and cortical bones in distal femurs as measured by peripheral quantitative CT. *B* shows the microCT images and the quantitative measurements of trabecular bones (*Tb.V.*) in the distal femurs of wild-type and *Ccr1$^{-/-}$* mice (*n* = 10). In *C–F*, the bone histomorphometric analyses of distal femurs in wild-type and *CCR1$^{-/-}$* mice were carried out as described under "Experimental Procedures." Parameters relating to the trabecular structure (in *C*): bone volume per tissue volume (*BV/TV*), trabecular number (*Tb.N.*), and trabecular separation (*Tb.Sp.*). Parameters relating to bone formation (in *D*): osteoid volume to bone volume (*OV/BV*), osteoid surface/bone surface (*OS/BS*), osteoid thickness (*O.Th.*), formation rate referenced to bone surface (*BFR/BS*), mineral apposition rate (*MAR*), and mineralizing surface per bone surface (*MS/BS*). The immunofluorescence images of calcein labeling in wild-type and *Ccr1$^{-/-}$* mice (in *E*). Parameters relating to bone resorption (in *F*): osteoclast number per bone perimeter (*N.Oc./B.Pm*), osteoclast surface per bone surface (*Oc.S./BS*), eroded surface per bone surface (*ES/BS*), and osteoblast surface per bone surface (*Ob.S./BS*). The bone histomorphometric analysis data are represented as the mean ± S.E. obtained from six mice in each group. #, significantly different from wild-type controls, *p* < 0.05. In *G*, osteocyte numbers per area are represented as the mean ± S.E. obtained from three mice in each group.

density in cancellous bone in *Ccr1$^{-/-}$* mice compared with wild-type mice (Fig. 1*A*). There were no significant differences between bone mineral density in the cortical bone at the metaphysial (Fig. 1*A*) and diaphysial regions (data not shown) between *Ccr1*-deficient and wild-type mice. In *Ccr1$^{-/-}$* mice, a microCT analysis indicated decreased cancellous bone tissue at the metaphysical region (Fig. 1*B*). An analysis of bone histomorphometrics confirmed a significant decrease of bone volume (*BV/TV*) at the metaphysial region of *Ccr1$^{-/-}$* mice. This was associated with a diminished number of trabeculae (*Tb.N*), increased trabecular bone separation (*Tb.Sp*), and no significant changes in trabecular bone thickness (*Tb.Th*), thus indicating that *Ccr1*-deficient mice have sparse trabeculae (Fig. 1*C*). We examined the effect of *Ccr1* deficiency on the function of osteoblasts and osteoclasts in bone morphometry (Fig. 1, *D–F*). The morphological analyses revealed that *Ccr1$^{-/-}$* mice have a significantly reduced number of osteoblasts (*Ob.S./BS*) (Fig. 1*F*). *Ccr1$^{-/-}$* mice exhibited extremely low values of osteoid surface (*OS/BS*) and osteoid volume (*OV/BV*) compared with wild-type mice (Fig. 1*D*). Notably, *Ccr1$^{-/-}$* mice showed a sig-

nificant decreases in the mineral apposition rate (*MAR*), mineralized surface (*MS/BS*), and bone formation rate (*BFR/BS*) (Fig. 1*D*), which were calculated based on calcein administration (*representative pictures* are shown in Fig. 1*E*). In addition, the number of osteocytes per area was significantly reduced in *Ccr1$^{-/-}$* mice (Fig. 1*G*). These results indicate that *Ccr1$^{-/-}$* mice have impaired bone formation. Fig. 1*F* summarizes the bone morphometric parameters associated with bone resorption. *Ccr1$^{-/-}$* mice have significantly decreased osteoclast numbers (*N.Oc./B.Pm*) and osteoclast surface area (*Oc.S./BS*), and an eroded surface (*ES/BS*). These findings indicate that *Ccr1$^{-/-}$* mice have diminished osteoclast function. Taken together, the morphometric analyses suggest that the bone phenotype in *Ccr1*-deficient mice exhibit osteopenia with low bone turnover, which is most likely due to the diminished function of osteoblasts and osteoclasts.

Impaired Osteogenesis and Osteoclastogenesis in the Bone Tissue of Ccr1-deficient Mice—To elucidate the status of osteoblasts and osteoclasts in bones of *Ccr1$^{-/-}$* mice, we compared the transcriptional levels of osteoclast- and osteoblast-related
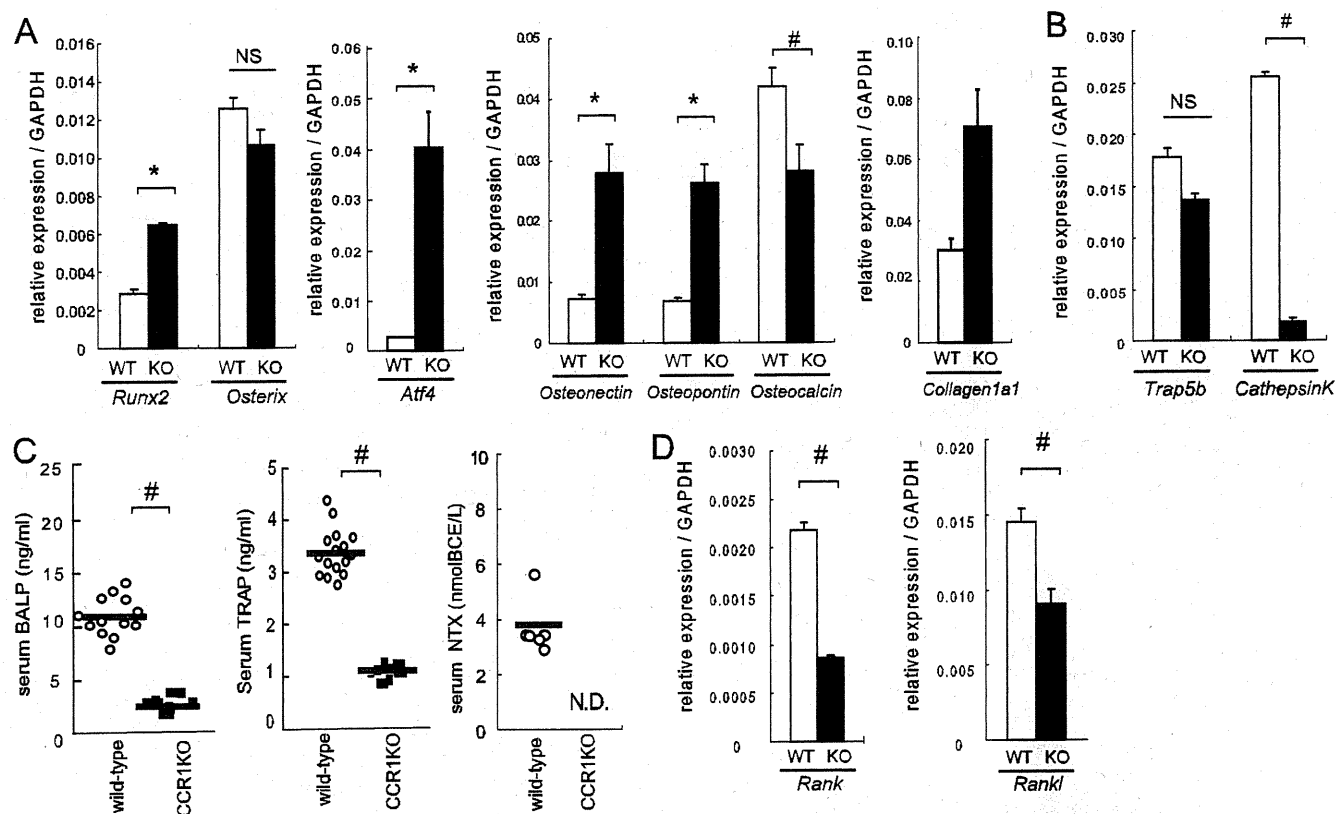
FIGURE 2. **Expression of markers related to osteoblasts and osteoclasts in bones and sera in wild-type and** $CCR1^{-/-}$ **mice.** In A, B, and D, total RNAs were isolated form the proximal tibia of wild-type and $Ccr1^{-/-}$ male mice at 8 weeks of age. Real-time Q-PCR revealed the relative expression levels of osteoblast-related mRNAs (Runx-2, Osterix, Atf4, Osteonectin, Osteopontin, Osteocalcin, and Collagen1α1, A), osteoclast-related mRNA (Trap5a and Cathepsin K, B), and RANK–RANKL axis (Rank and Rankl, D). Data are expressed as the copy numbers of these markers normalized to Gapdh expression (mean ± S.E., n = 8). In C, the levels of serum BALP, TRAP, and serum collagen-type1 N-telopeptides (NTx) were measured by ELISA. The bars indicate the mean ± S.E. Each sample was duplicated. Wild-type and $Ccr1^{-/-}$ male mice at 9 weeks of age (n = 10 and 6, respectively) were subjected to BALP and TRAP. Wild-type and $Ccr1^{-/-}$ male mice at 9–13 weeks of age (n = 8 and 6, respectively) were assayed for NTx. #, significantly different from wild-type controls, $p < 0.05$. N.D., not detected.

markers in the proximal tibiae of wild-type and $Ccr1^{-/-}$ mice. The analyses of osteoblast-related markers, such as bone-specific transcriptional factors (Runx-2, Atf4, and Osterix) (23–25) and bone matrix proteins (Collagen1a1, Osteonectin, Osteopontin, and Osteocalcin), revealed that the expression levels of Runx2 and Atf4 were dramatically up-regulated in $Ccr1^{-/-}$ mice than in wild-type mice (Fig. 2A). However, there were no significant changes in the expression levels of Osterix. Early markers for osteoblast differentiation, including Collagen1a1, Osteonectin, and Osteopontin, were significantly up-regulated. Osteocalcin expression, a marker for mature osteoblasts, was significantly down-regulated in $Ccr1^{-/-}$ mice. These results suggest that osteoblasts in Ccr1-deficient mice are retained in an immature state due to the overexpression of Runx-2 and Atf4 by osteoblasts, which is also consistent with the significant reduction in number of osteocytes in $Ccr1^{-/-}$ mice. Constitutive Runx-2 overexpression in osteoblasts results in maturation arrest in osteoblasts and in a reduced number of osteocytes (25). The serum levels of BALP in Ccr1-deficient mice were significantly decreased (Fig. 2C).

The expression levels of markers related to osteoclast differentiation, revealed attenuated transcription levels of TRAP5b and cathepsin K in $Ccr1^{-/-}$ mice (Fig. 2B). In addition, $Ccr1^{-/-}$ mice exhibited significantly decreased levels of serum TRAP (26) and collagen-type I NTx (27, 28) (Fig. 2C). This finding is

consistent with diminished osteoclastic bone resorption in $Ccr1^{-/-}$ mice. These observations led us to assess the RANK-RANKL axis, a key signaling pathway in osteoblast-osteoclast interactions that regulates osteoclast differentiation and function. Interestingly, the analyses revealed that both Rank and Rankl were down-regulated (Fig. 2D), thus implying that CCR1 is involved in the regulation of the RANK-RANKL axis. Considering the fact that $Ccr1^{-/-}$ mice exhibit osteopenia with low bone turnover, these bone cell marker expression levels suggest that CCR1 is heavily involved in the differentiation and function of osteoblasts and osteoclasts as well as in the cellular interactions between these cell types.

CCR1 Signaling Is Important in the Maturation and Function of Osteoblasts—To further corroborate the necessity of CCR1 in osteoblast maturation and function, we examined the formation of mineralized nodules in vitro by osteoblastic cells isolated from bone marrow of wild-type and $Ccr1^{-/-}$ mice. Mineralized nodule formation in osteoblastic cells isolated from $Ccr1^{-/-}$ mice was markedly abrogated compared with wild-type osteoblastic cells (Fig. 3A). We next investigated the time-course expression profiles of osteoblastic markers in this in vitro culture system and compared them between wild-type and $Ccr1^{-/-}$ mice (Fig. 3B). In wild-type mice, Runx2 exhibited the highest levels of expression at day 14, but was drastically down-regulated at day 21, during the mineralization stage. However,
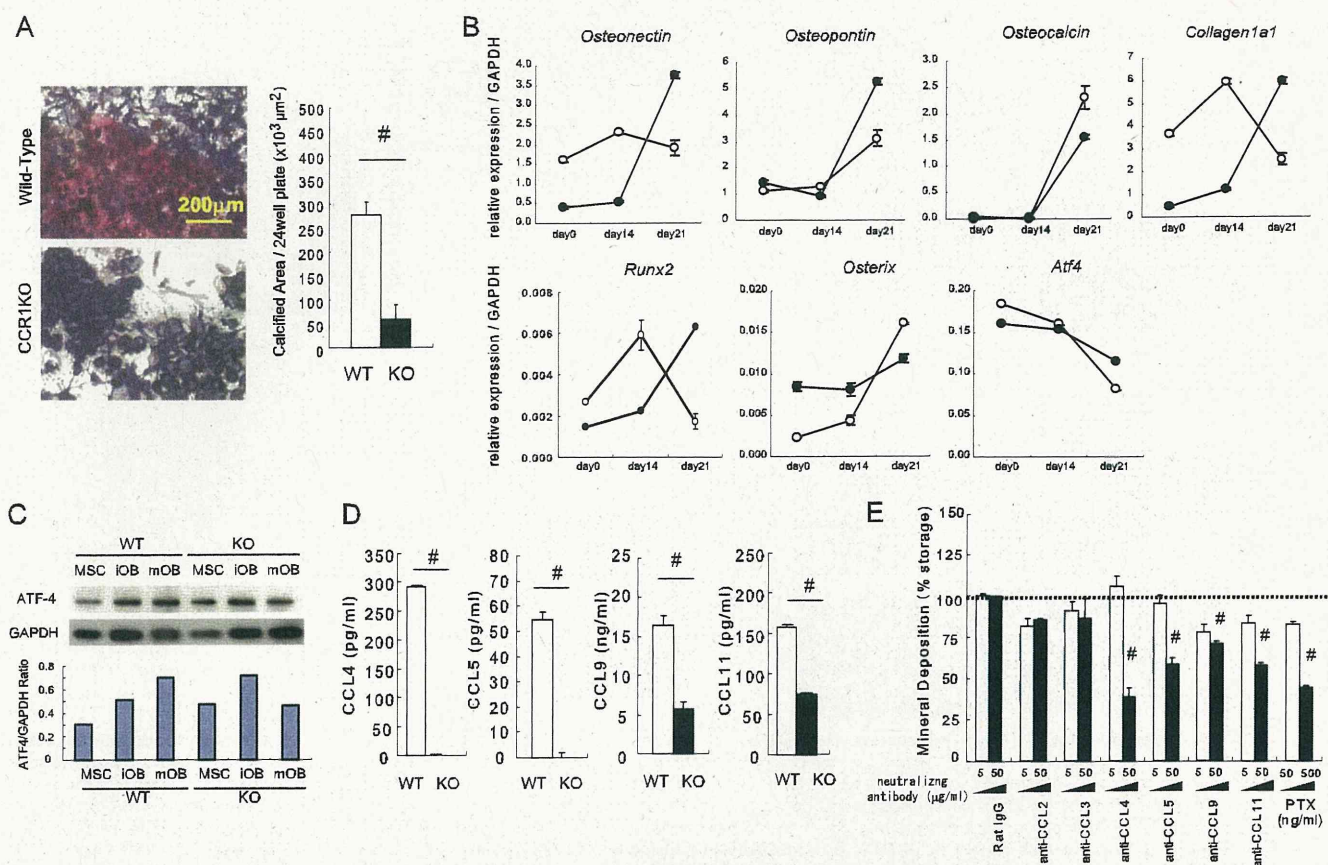
FIGURE 3. **Impaired mineralized nodule formation in *CCR1*-deficient osteoblastic cells.** In *A*, osteoblastic cells were cultured from the bone marrow of wild-type and *Ccr1*$^{-/-}$ mice, and then minerals were stained with alizarin red and BALP with chromogenic reagents (shown in *"blue"*) (magnification ×100, *left*). Mineral deposition was determined by von Kossa staining (*n* = 6, *right*). In *B*, total RNAs were isolated from osteoblastic cells isolated from wild-type (*open circles*) and *Ccr1*$^{-/-}$ mice (*filled circles*). The real-time Q-PCR analyses examined the relative expression levels of osteoblast-related transcriptional factor mRNAs (*Runx-2*, *Osterix*, and *Atf4*) and osteoblast-related marker mRNAs (*Osteonectin*, *Osteopontin*, *Osteocalcin*, and *Collagen1α1*). Data are expressed as the copy numbers of these markers normalized to *Gapdh* expression (mean ± S.E., *n* = 8). In *C*, the protein expression levels of the transcriptional factor ATF4 by wild-type and *Ccr1*$^{-/-}$ osteoblastic cells were measured by a Western blot analysis. Osteoblast lysates (10 μg of protein per lane) was loaded and separated by SDS-PAGE. The expression levels of ATF4 were normalized to GAPDH expression. In *D*, the production of CCR1-related chemokine ligands in the culture media of wild-type and *Ccr1*$^{-/-}$ osteoblastic cells was measured by ELISA (*n* = 5). #, significantly different from wild-type controls, *p* < 0.05. In *E*, osteoblastic cells were cultured with the indicated neutralizing antibodies against chemokines. The mineral deposition rate was measured by von Kossa staining (*n* = 4). Stained cells cultured with control rat IgG were set as 100%. #, significantly different from between different concentrations of each antibody, *p* < 0.05. *PTX*, pertussis toxin.

an inverse *Runx2* expression pattern was observed in CCR1-deficient osteoblastic cells, in which the levels of expression were markedly suppressed in the early stages (days 0 and 14), and was then significantly up-regulated at day 21, reaching the levels present in wild-type mice. *Osterix* expression was highly up-regulated at day 21 in wild-type mice, whereas its expression in CCR1-deficient osteoblastic cells was sustained at an intermediate level between the lowest and the highest levels in wild-type mice, overall resulting in a lower expression levels than in wild-type mice at day 21. These inverted expression patterns were also consistently observed, especially at day 21, with other osteoblastic markers, including *Atf4*, *Caollagen1a1*, *Osteonectin*, *Osteopontin*, and *Osteocalcin*. Similarly, the expression pattern of ATF4 was also confirmed by a Western blot analysis (Fig. 3*C*). These observations indicated that CCR1 deficiency severely affected the temporal expression of osteoblastic markers, resulting in the impaired differentiation and maturation of osteoblasts. Because CCR1 signaling is activated by several cross-reactive chemokines (CCL4, CCL5, CCL9, and CCL11), we next compared the levels of these chemokines in wild-type

and CCR1-deficient osteoblastic cells. We observed significantly diminished expression levels of these chemokines in *CCR1*-deficient osteoblastic cells (Fig. 3*D*). A test on the effects of neutralizing antibodies against various chemokines, including CCR1 ligands, revealed the role of each chemokine in mineralized nodule formation by osteoblastic cells. The neutralizing antibodies against CCL4, CCL5, CCL9, and CCL11 significantly reduced the number of mineralized nodules in osteoblastic cells, although the antibodies against CCL2 and CCL3 did not inhibit the numbers completely (Fig. 3*E*). Pertussis toxin (PTX), an inhibitor of G$_i$ protein-coupled receptors involved in chemokine signaling, inhibited mineralized nodule formation in a dose-dependent manner. In further support of these findings, we observed similar temporal changes in the transcriptional levels of osteoblastic markers in wild-type osteoblastic cultures treated with an anti-CCL9 antibody, compared with *Ccr1*$^{-/-}$ osteoblastic cells (supplemental Fig. 2). These results suggest that CCR1 signaling mediated by its ligands (CCL4, CCL5, CCL 9, and CCL11) plays an essential role in mineralized nodule formation.
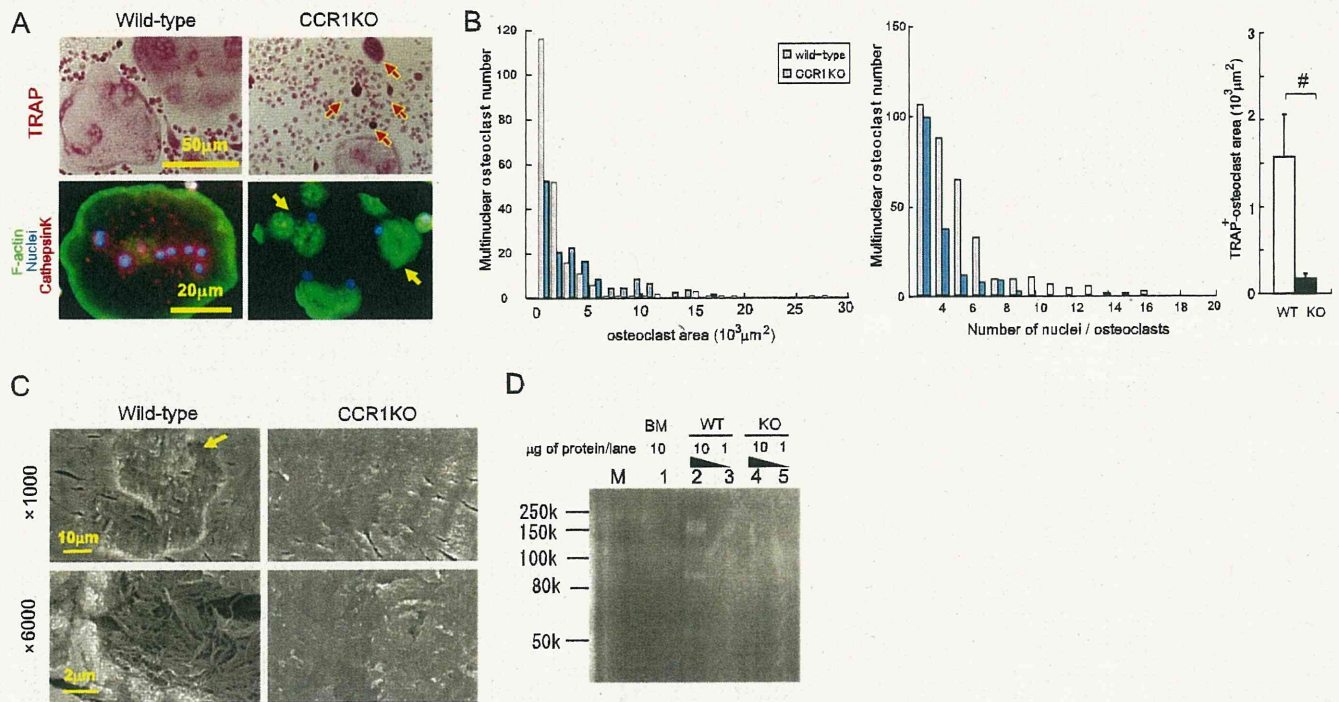
FIGURE 4. **Essential roles of CCR1 in multinucleation and bone-resorbing activity.** Pre-osteoclastic cells were cultured from the bone marrow of wild-type and $Ccr1^{-/-}$ mice. Osteoclasts were induced from the pre-osteoclastic cells by M-CSF and RANKL treatment. In A, the formation of multinuclear osteoclasts by wild-type and $Ccr1^{-/-}$ precursors was visualized by TRAP chromogenic staining (magnification ×400, *upper panels*). Immunohistochemical staining was carried out using an anti-cathepsin K antibody conjugated with Alexa594 (*red*). F-actin and nuclei were counterstained by phalloidin-AlexaFluor 488 (*green*) and Hoechst 33258 (*blue*), respectively (magnification ×640, *bottom panels*). The *yellow arrow* indicates multinuclear giant cells with an impaired actin ring rearrangement, and the *red arrows* indicate TRAP accumulation. In B, *histograms* of the area distribution of multinuclear osteoclasts delimited with phalloidin, and of the number of multinuclear osteoclasts in A. Area comprises TRAP-positive multinuclear (>3 nuclei) giant cells shown in A (mean ± S.E., n = 3). In C, pit formation by wild-type and $Ccr1^{-/-}$ osteoclasts on bone slice observed by scanning electron microscopy (magnification: ×1000 (*top*) and ×6000 (*bottom*), respectively). In D, collagen digestion activity by wild-type and $Ccr1^{-/-}$ osteoclasts was measured by collagen-based zymography. *Lanes M, 1, 2–3,* and *4–5* indicate the molecular markers, bone marrow-derived macrophage lysates (10 μg of protein/lane), wild-type osteoclast lysates (1 and 10 μg of protein/lane), and $Ccr1^{-/-}$ osteoclasts lysates (1 and 10 μg of protein/each lane), respectively.

Lack of Chemokine Receptor CCR1 Causes Impaired Osteoclast Differentiation and Bone-resorbing Activity—To elucidate the roles of CCR1 in osteoclast differentiation, we analyzed the differentiation potency of osteoclast precursors derived from $Ccr1^{-/-}$ mice (Fig. 4A). Osteoclast precursors from $Ccr1$-deficient mice markedly abrogated multinucleation with defective actin ring formation (Fig. 4A, *yellow arrows*) compared with precursors from wild-type mice, which generated a large numbers of osteoclasts with multinucleation and well organized actin ring formation at the cell periphery. The histograms of the osteoclast area and number of nuclei per cell as well as TRAP-positive areas reveal the presence of impaired cellular fusion and differentiation in $Ccr1$-deficient osteoclasts (Fig. 4B). We further investigated the activity of bone resorption in $Ccr1$-deficient osteoclasts (Fig. 4C). Few resorption pits were observed in $Ccr1^{-/-}$ osteoclasts by scanning electron microscopic examination, in contrast to obvious resorption pits with well digested collagen fibers detected in wild-type osteoclasts. This observation was also confirmed by collagen zymography demonstrating that $Ccr1^{-/-}$ osteoclasts failed to digest type-I collagens (Fig. 4D).

Furthermore, the transcriptional levels of osteoclastic differentiation markers were investigated in the osteoclast culture system. *Rank* and its downstream targets *Nfat-c1*, other markers such as c-*fos*, *Trap*, *CathepsinK*, *Atp6v0d2*, *integrin* αV, and *integrin* β3 were markedly down-regulated in $Ccr1$-deficient cells, whereas $S1P_1$ and *Irf-8* were up-regulated (Fig. 5A). We next examined whether the down-regulation in RANK expression *in vivo* (see Fig. 2D) and *in vitro* (Fig. 5A) directly correlated with the reduction in RANK-expressing osteoclast precursors. The cellular profiles of osteoclast precursors by a flow cytometric analysis revealed that the $Ccr1^{-/-}$ mice had lower numbers of CD45$^+$CD11b$^+$CD115$^+$ myeloid-lineage precursors compared with wild-type mice (Fig. 5B). In addition, the subpopulations of osteoclast precursors, which are categorized into CD11b^{hi} (R1) and CD11b^{lo} (R2), were marked reduced in the R2 subpopulation in CCR1-deficient cells. Because the R1 and R2 subpopulations reportedly express higher and lower levels of RANK, respectively (29), a reduction in the R2 subpopulation likely contributed to reduced expression of osteoclast markers in CCR1-deficient osteoclastic cells. Importantly, our observation is also consistent with a previous work reporting that RANK^{lo} precursors are required for cellular fusion (29).

CCR1 Signaling Is Involved in Osteoclast Differentiation—To further explore the role of CCR1 signaling in osteoclast differentiation, we next examined the expression levels of chemokine receptors during osteoclastogenesis using an *in vitro* culture system. CCR1 was expressed in the course of the osteoclastogenesis, with the highest levels of expression at day 4 after culture (10–12), whereas other chemokine receptor CCR2 was gradually down-regulated during this culture period (30)
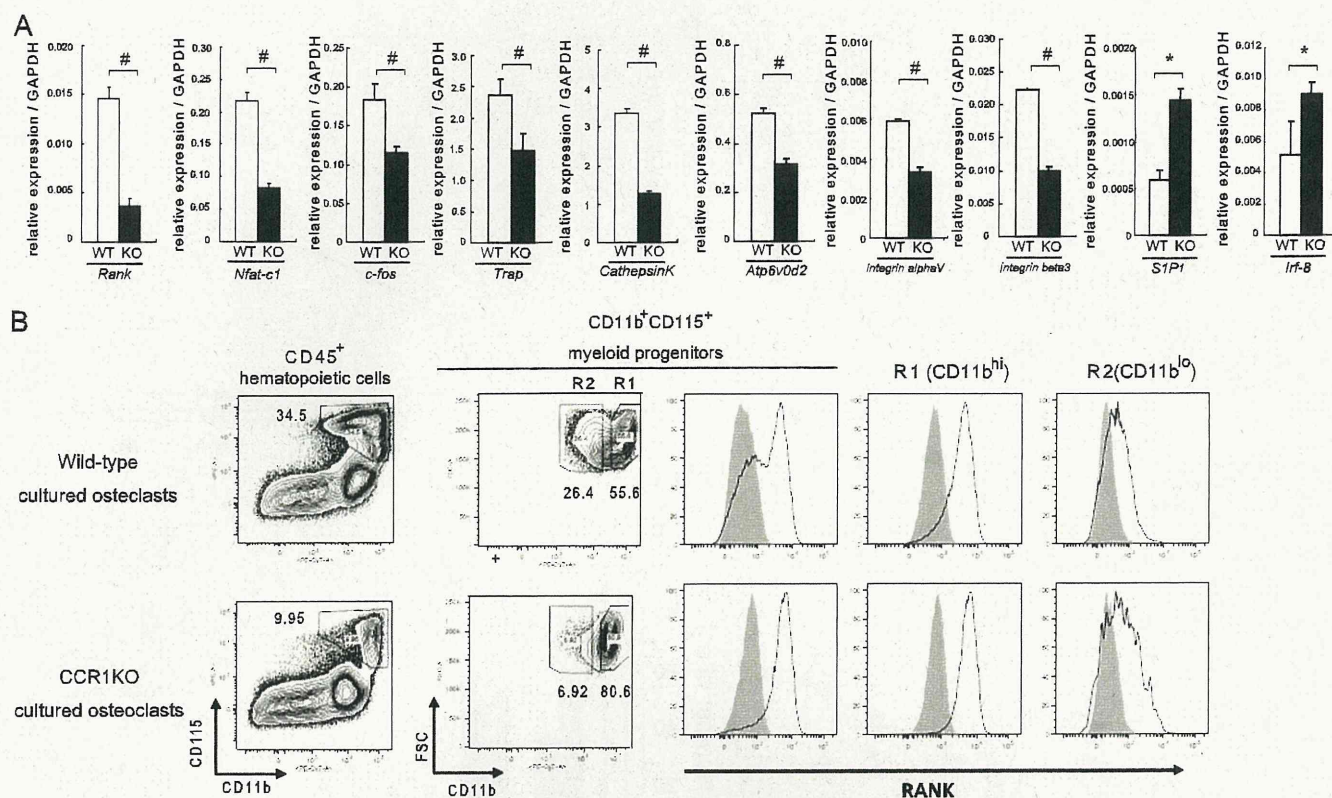
FIGURE 5. **Osteoclastic impairment by CCR1 deficiency is due to the changes in osteoclastic precursor population.** Pre-osteoclastic cells were cultured from the bone marrow of wild-type and $Ccr1^{-/-}$ mice. Osteoclasts were induced from the pre-osteoclastic cells by M-CSF and RANKL treatment. In A, relative expression levels of the osteoclastic differentiation markers (*Rank*, *Nfatc1* transcription factor, *c-fos*, *Trap*, *CathepsinK* protease, H^+-ATPase subunit *ATP6v0d2*, integrins αV and $\beta 3$, *S1P_1*, and *Irf-8*) on wild-type (*open column*) and $Ccr1^{-/-}$ (*filled column*) osteoclasts were measured by a real-time Q-PCR analysis at day 4 after culture (mean ± S.E., $n = 5$). #, significantly different from wild-type controls, $p < 0.05$. In B, expression analysis of RANK in $CD45^+CD11b^+CD115^+$ pre-osteoclastic cells isolated from the bone marrows of wild-type and $Ccr1^{-/-}$ mice after 4 days in culture were analyzed by flow cytometry.

(Fig. 6A). Immunohistochemical staining revealed that CCR1 was highly expressed on the multinuclear osteoclasts (supplemental Fig. 3). The expression profiles of CCR ligands in this *in vitro* osteoclast culture system revealed that ligands specific for CCR1, such as *Ccl5* and *Ccl9*, had a relatively higher levels of expression than other ligands, and appeared to be regulated depending on the maturation stages of the osteoclasts. *Ccl5* was preferentially expressed at day 4, a stage of mononuclear pre-osteoclasts, whereas multinuclear osteoclasts predominantly produced *Ccl9* at later times (Fig. 6B). These regulated transcriptional patterns of *Ccl5* and *Ccl9* were also confirmed by the analysis of protein expression levels in cultured media (Fig. 6C). These observations suggested that the interaction between CCR1 and its ligands, CCL5 and CCL9, could be involved in osteoclast differentiation.

We verified this hypothesis by culturing osteoclast precursors in the presence of neutralizing antibodies against CCL5 and CCL9. Blockade of either ligand resulted in a partial inhibition of osteoclast formation in a dose-dependent manner. Similarly, simultaneous treatment with neutralizing antibodies against CCL5 and CCL9 induced synergistic inhibitory effects (Fig. 6D). Furthermore, PTX treatment blocked osteoclastogenesis to the basal levels. Notably, we found no CCL3 production by ELISA or any inhibitory osteoclastogenesis effects using an anti-CCL3 antibody (data not shown), although CCL3 is thought to play an essential role in inflammation-related oste-

oclastogenesis in humans (4, 7, 31, 32). These findings indicate that CCR1 is essential for osteoclast differentiation, and CCL5 and CCL9 are the likely candidate ligands that participate in the CCR1 axis.

CCR1 Is Involved in the RANK–RANKL Axis and Induces the Impaired Osteoclastogenesis—Because osteoclast differentiation is critically regulated by the signals through the RANK–RANKL axis, we investigated the transcriptional level of *Rankl* in $Ccr1^{-/-}$ osteoblastic cells. The cells expressed significantly lower levels of RANKL compared with wild-type osteoblastic cells (Fig. 7A). We next performed co-cultures of pre-osteoclasts with layers of osteoblastic cells by reciprocal combinations of these two cell populations from wild-type and $Ccr1^{-/-}$ mice. As expected from the reduced *Rankl* expression, a significantly reduced number of osteoclasts were formed from co-culture with $Ccr1^{-/-}$ osteoblastic cells compared with wild-type osteoblastic cells (Fig. 7B). In the presence of PTX, wild-type osteoblastic cells also failed to generate substantial numbers of osteoclasts (Fig. 7B). $Ccr1^{-/-}$ osteoclast precursors did not form differentiated osteoclasts even in the presence of wild-type-derived osteoblasts (Fig. 7C), as is consistent with our observations in Fig. 4. These observations suggest that the CCR1 chemokine receptor, which is expressed by both osteoblasts and osteoclasts, plays a critical role on osteoblast-osteoclast communication through the regulation of the RANK and RANKL expression.
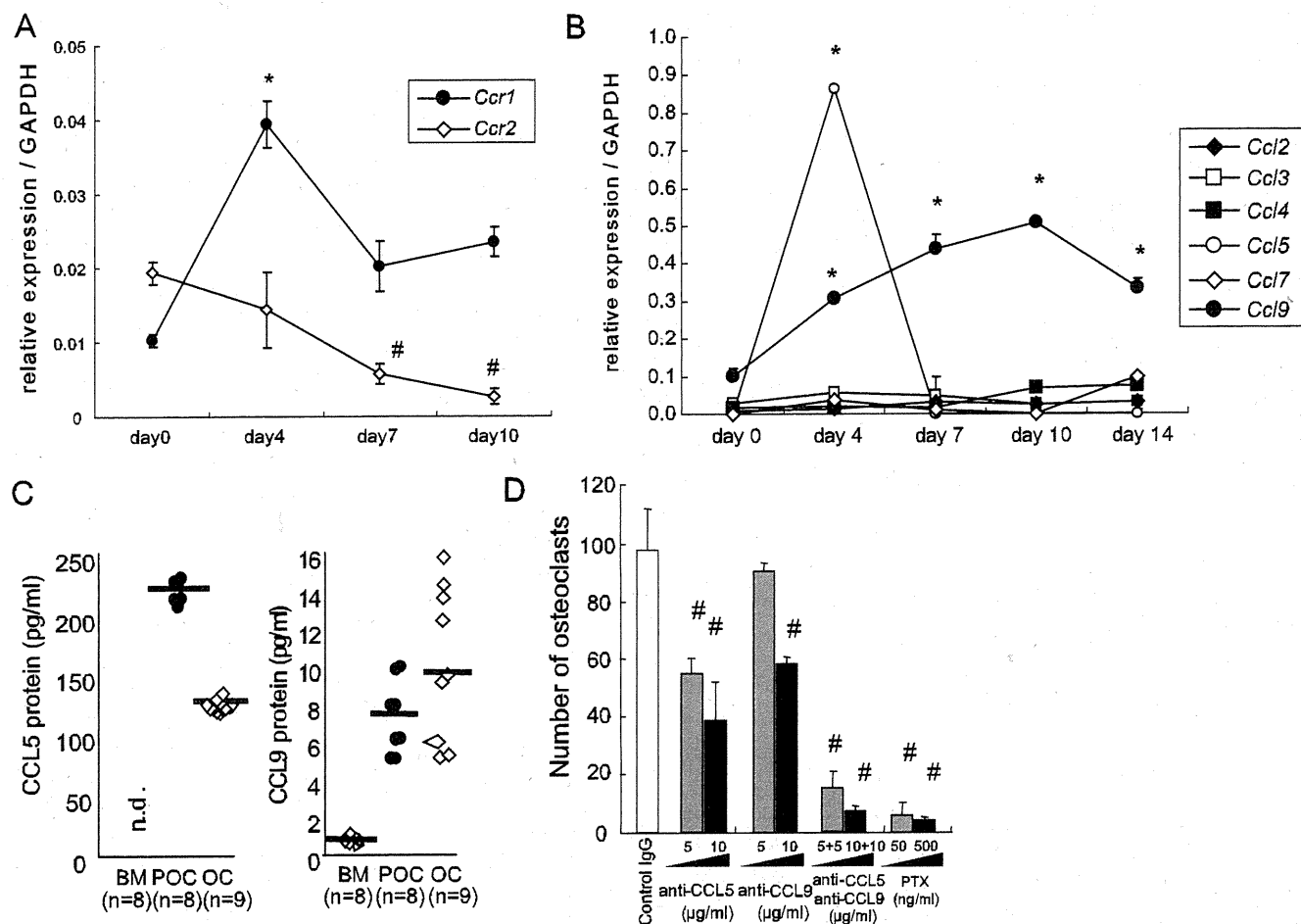
FIGURE 6. **CCR1 signaling is involved in osteoclast differentiation.** Osteoclastic cells and macrophages were cultured from the bone marrow of wild-type and $Ccr1^{-/-}$ mice. Total RNAs were isolated from the cultured cells. The relative mRNA expression levels of chemokine receptors $Ccr1$, $Ccr2$ (A) and chemokine ligands (B) during osteoclastogenesis were measured by real-time Q-PCR (mean ± S.E., $n = 5$). * and #, significantly different from day 0 of $Ccr1$ and $Ccr2$, respectively, $p < 0.05$ in A. *, significantly different from day 0 of culture in each ligand expression, $p < 0.05$ in B. In C, chemokine levels during osteoclastogenesis were measured by ELISA. BM, bone marrow-derived macrophage; POC, pre-osteoclast (day 4); and OC, osteoclast (day14). Bars indicate the mean. In D, the number of osteoclasts after neutralization of CCL5, CCL9, and their combination in the osteoclastic cultures were scored (mean ± S.E., $n = 3$). #, significantly different between two distinct concentrations of each antibody, $p < 0.05$. PTX, pertussis toxin.

DISCUSSION

Pathological findings postulate that chemokines and chemokine receptors are involved in bone remodeling (9–13). Among these receptors, CCR1 appears to be an important molecule involved in bone metabolism (9). We used $Ccr1^{-/-}$ mice to investigate whether CCR1 affects bone metabolism. Our findings have demonstrated that a CCR1-deficiency affects the differentiation and function of both osteoblasts and osteoclasts, and also causes osteopenia.

Our bone histomorphometric study in $Ccr1^{-/-}$ mice clearly demonstrated impaired osteoblast differentiation and function (Fig. 1, *D–G*). The bone tissues in $Ccr1^{-/-}$ mice exhibited down-regulation of *osteocalcin*, which is a marker for mature osteoblasts, whereas the expression of *Osteonectin* and *Osteopontin*, which are markers for early osteoblasts, were up-regulated in the bones of these mice (Fig. 2*A*). Significantly, $Ccr1^{-/-}$ osteoblastic cells exhibited much less potency to generate mineralized tissues (Fig. 3*A*). These results suggest that the deficiency of CCR1 results in arrested osteoblast maturation and defective osteoblast function. Previous reports have

demonstrated that the sustained expression of *Runx2* in osteoblasts inhibits their terminal maturation and causes osteopenia with a reduction in the number of osteocytes (25, 33). Consistent with these findings, bone tissue specimens from $Ccr1^{-/-}$ mice exhibited a higher expression level of *Runx2* and a reduced number of osteocytes (Fig. 3*G*). These findings suggest that osteopenia in $Ccr1^{-/-}$ mice is due to impaired osteoblastic function via *Runx2* up-regulation. Our findings in $Ccr1^{-/-}$ osteoblastic culture supportively demonstrated that an inverse temporal expression level of osteoblastic transcriptional factors, such as *Runx2*, *Atf4*, and *Osterix* could be related to the disordered expressions of bone matrix proteins, thus resulting in impaired bone mineral deposition (Fig. 3*B*).

Furthermore, treatment with neutralizing antibodies against CCR1 ligands (*e.g.* CCL4, CCL5, CCL9, and CCL11) significantly inhibited mineral deposition (Fig. 3*E*) and osteoblastic protein expression (supplemental Fig. 2) in osteoblastic cells isolated from wild-type mice. These observations indicate that CCR1-mediated signaling is essential for osteoblast differentiation and function. Although we detected substantial levels of
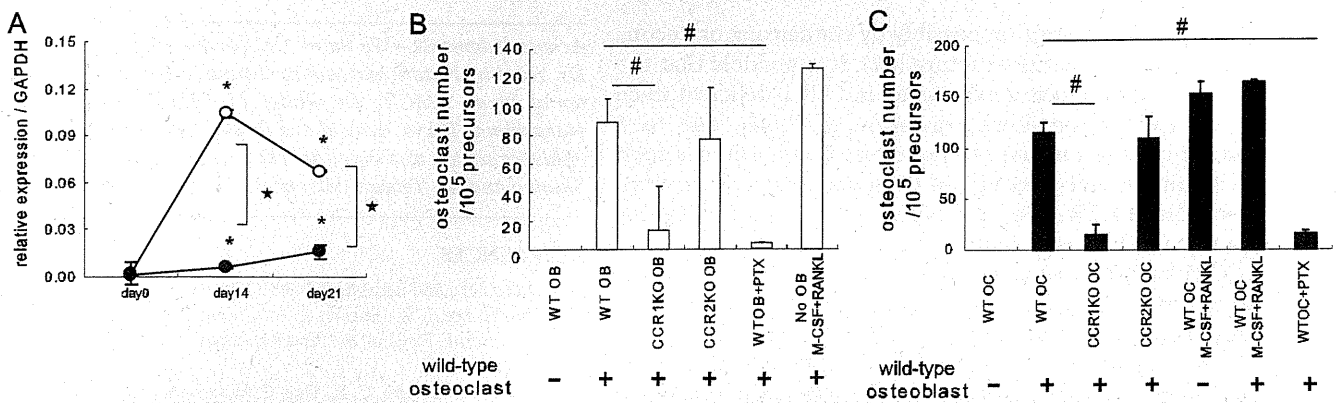
FIGURE 7. **CCR1 is involved in the RANK–RANKL axis and induces the impaired osteoclastogenesis.** In A, osteoblastic cells were cultured from the bone marrow of wild-type and $Ccr1^{-/-}$ mice. Relative expression levels of $Rankl$ by $Ccr1^{-/-}$ osteoblasts as measured by real-time Q-PCR (mean ± S.E., n = 3). [#], significantly different from wild-type controls, $p < 0.05$. In B and C, the number of TRAP[+] multinuclear osteoclasts induced by co-culture with osteoblasts. Co-culture with osteoblastic cells isolated from wild-type or $Ccr1^{-/-}$ mice (mean ± S.E., duplicated, n = 2, B), and with osteoclast precursors isolated from wild-type or $Ccr1^{-/-}$ mice (mean ± S.E., duplicated, n = 2, C). Osteoclast cultures with M-CSF and RANKL without osteoblasts were set as positive control. [#], significantly different from co-culture of osteoclasts with wild-type osteoblasts, $p < 0.05$.

various chemokine ligands (CCL4, CCL5, CCL9, and CCL11) in osteoblastic cells, these levels were greatly reduced in cells isolated from $Ccr1^{-/-}$ mice (Fig. 3D). This observation implies a chemokine-dependent amplification loop by which a given chemokine signaling sustains or amplifies the expressions of its participating ligands and receptors, which has been previously reported in several contexts. For instance, the activation of CD14^{+} monocytes form a CCR2-CCL2 axis-dependent amplification loop that ultimately leads to fibrosis (34). Several other studies have reported that macrophage infiltration in injured tissue is mediated by a CCR1-mediated loop (35–37) and a CCR5–CCL5 loop (38). Reports of renal inflammatory signals and abdominal inflammation have described CCR7–CCL19/CCL21 (39) and CCR8–CCL1 loops (17), respectively. Therefore, the CCR1-mediated loop is likely to be involved in osteoblast differentiation, function, and cellular interactions that regulate bone metabolism. Possible roles of the CCR1-mediated loop in osteoblast differentiation and function suggest that changes in the bone marrow microenvironment by a CCR1 deficiency affected the osteoblastic lineage and/or the intercellular regulation of osteoblast differentiation and function. CCR1 conventional knock-down seems to have affected many cell types that express CCR1, affecting the bone marrow microenvironment, which regulates whole process of osteoblast differentiation and function. Our *in vitro* experiments did not successfully retrieve this point. Nevertheless, the present experiments have confirmed an essential role for CCR1-mediated signaling in osteoblastic cells. The expression and possible roles of CCR1 in osteoclast lineage cells have been reported by several studies (4, 10, 11). We observed the up-regulation of $Ccr1$ expression and down-regulation of $Ccr2$ during cultured osteoclastogenesis (Fig. 6A). The bone histomorphometric analyses demonstrated impaired osteoclast differentiation and function in $Ccr1^{-/-}$ mice (Fig. 1F). In addition, we observed impaired bone resorption activity by osteoclasts isolated from $CCR1^{-/-}$ mice (Fig. 4, B and C). A potential reason for the impaired bone resorption is due to defects in osteoclast differentiation. Indeed, the flow cytometric analyses revealed that the component of CD11b^{+}CD115^{+} myeloid-lineage pre-

cursors in $Ccr1^{-/-}$ mice are drastically changed; this population of cells lacked the RANK^{lo} CD11b^{lo} subpopulation, which is required for cellular fusion (29) (Fig. 5B). Recent live observation of calvarial bone marrow by two-photon microscopy clarified the roles of chemoattractant S1P$_1$ (sphingosine-1-phosphate 1) and its receptors in the migration of osteoclast precursors to the bone surface (40). Therefore, it is indeed intriguing to speculate that elevated levels of $S1P_1$ expression in $Ccr1^{-/-}$ osteoclasts (Fig. 1F) reduced the supply of osteoclast precursors from peripheral circulation in the bone marrow to the bone surface. Further investigation will reveal whether the CCR1 axis is involved in the chemotactic migration of osteoclast precursors to the bone surface.

One of the possible reasons for osteoclast dysfunction in $Ccr1^{-/-}$ mice may be diminished signaling along the RANK–RANKL axis. The down-regulation of both $Rank$ and $Rankl$ mRNA was observed in the bone tissue of $Ccr1^{-/-}$ mice (Fig. 2D). Cultured osteoblastic cells and osteoclasts isolated from $Ccr1^{-/-}$ mice exhibited remarkable reductions in $Rank$ and $Rankl$ expression levels, respectively (Figs. 5B and 7B). Furthermore, $Ccr1$-deficient osteoclasts had discouraged the levels of osteoclastic maturation markers such as c-*fos*, *Nfatc1*, *Cathepsink*, and several integrins (Fig. 5A). These results suggest that CCR1-mediated signaling controls the RANK–RANKL axis through the regulation of both osteoblasts and osteoclasts. Our intercross co-cultures of pre-osteoclasts with osteoblastic cells from wild-type and $Ccr1^{-/-}$ mice obviously demonstrated an impaired interaction between these two cell types, resulting in the impaired induction of functional mature osteoclasts (Fig. 7, B and C). These findings, interestingly, support the idea that the chemokines produced by the osteoblasts and osteoclasts that stimulate CCR1-mediated signaling could be categorized as putative "bone-coupling factors" (41), which mediate the cross-talk between osteoclasts and osteoblasts to maintain bone remodeling.

Our data imply that the regulatory mechanism of $Rankl$ expression is associated with osteoblast maturation. Runx2 reportedly induce a low steady-state level of $Rankl$ expression and is also required for the stimulatory effect of vitamin

Role of CCR1 in Bone Metabolism

D_3 on *Rankl* transcription possibly by condensing or decondensing the chromatin structure (42). It is possible that the inverse-temporal *Runx2* expression in CCR1-deficient mice is causative of the down-regulation of *Rankl*, due to a reduced cellular response to bone-targeted hormones such as vitamin D_3 and parathyroid hormone. However, a more direct role of CCR1-mediated signaling on *Rankl* transcription remains to be elucidated.

CCR1-mediated signaling pathways on both osteoblasts and osteoclasts raise important questions on how the several members of murine chemokine ligands for CCR1 (in rodents, CCL3, CCL4, CCL5, CCL6, CCL8, CCL9, and CCL11) (43) distinguish the downstream signaling pathways, despite sharing the same CCR1 receptor. Each chemokine may possess specific regulatory control for binding to the receptor and inducing a specific cellular response. For example, the osteoclasts may have a distinct intrinsic signaling adaptor protein for cellular response, as well as the adaptor protein FROUNT for CCR2-mediated signaling (44). It has also been demonstrated that the spatiotemporal expression of chemokine receptors and their ligands may relay chemokine signaling and sequential output that regulate bone metabolism. This is related to several findings in this study, including the distinct temporal expression patterns of different ligands as observed in Fig. 6 (*B* and *C*) and supplemental Fig. 1, the chemokine-dependent amplification loop, and the possible chemokine-mediated cellular interaction. Further studies are warranted to investigate the intracellular signaling pathways downstream of each chemokine receptor.

Our current results also support the concept that chemokine receptor antagonists are potentially novel therapeutic candidates for the treatment of patients with certain inflammatory bone diseases. Several reports suggest that CCL3 promotes pathological bone destruction by excessively triggering osteoclast activation (2, 4, 7, 31, 32). However, we were unable to detect increased CCL3 production by cultured osteoclasts (Fig. 6, *B* and *C*, and data not shown), suggesting that physiological osteoclastogenesis is primarily maintained by CCL9 rather than CCL3. It is probable that pro-inflammatory CCL3 overcomes the physiological process of osteoclastogenesis by CCL9 expression and signaling, thereby inducing ectopic osteoclastogenesis that causes bone destruction mediated by T-lymphocyte-mediated activation (45). Alternatively, the species differences between rodents and humans must be considered; CCL9 is described only in rodents, and the putative human homologue is predicted to be CCL15 and CCL23 (46), which are potent osteoclastogenesis mediators in humans (47). It is therefore worthwhile to dissect the distinct roles of chemokine signaling in both the pathological and physiological contexts, which would provide novel information that may help researchers identify new therapeutic targets.

In conclusion, the present observations provide the first evidence for the physiological roles of CCR1-mediated chemokines in the bone metabolism. Further studies on chemokine receptors in the bone metabolism will enable the targeted development of new therapeutic strategies for the treatment of patients with bone destruction diseases and osteoporosis.

REFERENCES

1. Charo, I. F., and Ransohoff, R. M. (2006) *N. Engl. J. Med.* **354,** 610–621
2. Oba, Y., Lee, J. W., Ehrlich, L. A., Chung, H. Y., Jelinek, D. F., Callander, N. S., Horuk, R., Choi, S. J., and Roodman, G. D. (2005) *Exp. Hematol.* **33,** 272–278
3. Kim, M. S., Magno, C. L., Day, C. J., and Morrison, N. A. (2006) *J. Cell Biochem.* **97,** 512–518
4. Menu, E., De Leenheer, E., De Raeve, H., Coulton, L., Imanishi, T., Miyashita, K., Van Valckenborgh, E., Van Riet, I., Van Camp, B., Horuk, R., Croucher, P., and Vanderkerken, K. (2006) *Clin. Exp. Metastasis* **23,** 291–300
5. Haringman, J. J., Smeets, T. J., Reinders-Blankert, P., and Tak, P. P. (2006) *Ann. Rheum. Dis.* **65,** 294–300
6. Choi, S. J., Cruz, J. C., Craig, F., Chung, H., Devlin, R. D., Roodman, G. D., and Alsina, M. (2000) *Blood* **96,** 671–675
7. Han, J. H., Choi, S. J., Kurihara, N., Koide, M., Oba, Y., and Roodman, G. D. (2001) *Blood* **97,** 3349–3353
8. Vallet, S., Raje, N., Ishitsuka, K., Hideshima, T., Podar, K., Chhetri, S., Pozzi, S., Breitkreutz, I., Kiziltepe, T., Yasui, H., Ocio, E. M., Shiraishi, N., Jin, J., Okawa, Y., Ikeda, H., Mukherjee, S., Vaghela, N., Cirstea, D., Ladetto, M., Boccadoro, M., and Anderson, K. C. (2007) *Blood* **110,** 3744–3752
9. Yang, M., Mailhot, G., MacKay, C. A., Mason-Savas, A., Aubin, J., and Odgren, P. R. (2006) *Blood* **107,** 2262–2270
10. Yu, X., Huang, Y., Collin-Osdoby, P., and Osdoby, P. (2004) *J. Bone Miner. Res.* **19,** 2065–2077
11. Lean, J. M., Murphy, C., Fuller, K., and Chambers, T. J. (2002) *J. Cell Biochem.* **87,** 386–393
12. Okamatsu, Y., Kim, D., Battaglino, R., Sasaki, H., Spate, U., and Stashenko, P. (2004) *J. Immunol.* **173,** 2084–2090
13. Kominsky, S. L., Abdelmagid, S. M., Doucet, M., Brady, K., and Weber, K. L. (2008) *Cancer Res.* **68,** 1261–1266
14. Binder, N. B., Niederreiter, B., Hoffmann, O., Stange, R., Pap, T., Stulnig, T. M., Mack, M., Erben, R. G., Smolen, J. S., and Redlich, K. (2009) *Nat. Med.* **15,** 417–424
15. Gao, J. L., Wynn, T. A., Chang, Y., Lee, E. J., Broxmeyer, H. E., Cooper, S., Tiffany, H. L., Westphal, H., Kwon-Chung, J., and Murphy, P. M. (1997) *J. Exp. Med.* **185,** 1959–1968
16. Doi, M., Nagano, A., and Nakamura, Y. (2002) *Biochem. Biophys. Res. Commun.* **290,** 381–390
17. Hoshino, A., Kawamura, Y. I., Yasuhara, M., Toyama-Sorimachi, N., Yamamoto, K., Matsukawa, A., Lira, S. A., and Dohi, T. (2007) *J. Immunol.* **178,** 5296–5304
18. Ito, M., Ikeda, K., Nishiguchi, M., Shindo, H., Uetani, M., Hosoi, T., and Orimo, H. (2005) *J. Bone Miner. Res.* **20,** 1828–1836
19. Parfitt, A. M., Drezner, M. K., Glorieux, F. H., Kanis, J. A., Malluche, H., Meunier, P. J., Ott, S. M., and Recker, R. R. (1987) *J. Bone Miner. Res.* **2,** 595–610
20. Liotta, L. A., and Stetler-Stevenson, W. G. (1990) *Semin. Cancer Biol.* **1,** 99–106
21. Gogly, B., Groult, N., Hornebeck, W., Godeau, G., and Pellat, B. (1998) *Anal. Biochem.* **255,** 211–216
22. Wilson, M. J., Strasser, M., Vogel, M. M., and Sinha, A. A. (1991) *Biol. Reprod.* **44,** 776–785
23. Komori, T., Yagi, H., Nomura, S., Yamaguchi, A., Sasaki, K., Deguchi, K., Shimizu, Y., Bronson, R. T., Gao, Y. H., Inada, M., Sato, M., Okamoto, R., Kitamura, Y., Yoshiki, S., and Kishimoto, T. (1997) *Cell* **89,** 755–764
24. Ducy, P., Zhang, R., Geoffroy, V., Ridall, A. L., and Karsenty, G. (1997) *Cell* **89,** 747–754

25. Liu, W., Toyosawa, S., Furuichi, T., Kanatani, N., Yoshida, C., Liu, Y., Himeno, M., Narai, S., Yamaguchi, A., and Komori, T. (2001) *J. Cell Biol.* **155**, 157–166

26. Delmas, P. D. (1993) *J. Bone Miner. Res.* **8**, Suppl. 2, S549–S555

27. Takahashi, M., Kushida, K., Hoshino, H., Ohishi, T., and Inoue, T. (1997) *J. Endocrinol. Invest* **20**, 112–117

28. Schneider, D. L., and Barrett-Connor, E. L. (1997) *Arch. Intern. Med.* **157**, 1241–1245

29. Arai, F., Miyamoto, T., Ohneda, O., Inada, T., Sudo, T., Brasel, K., Miyata, T., Anderson, D. M., and Suda, T. (1999) *J. Exp. Med.* **190**, 1741–1754

30. Saitoh, Y., Koizumi, K., Sakurai, H., Minami, T., and Saiki, I. (2007) *Biochem. Biophys. Res. Commun.* **364**, 417–422

31. Abe, M., Hiura, K., Wilde, J., Moriyama, K., Hashimoto, T., Ozaki, S., Wakatsuki, S., Kosaka, M., Kido, S., Inoue, D., and Matsumoto, T. (2002) *Blood* **100**, 2195–2202

32. Chintalacharuvu, S. R., Wang, J. X., Giaconia, J. M., and Venkataraman, C. (2005) *Immunol. Lett.* **100**, 202–204

33. Kanatani, N., Fujita, T., Fukuyama, R., Liu, W., Yoshida, C. A., Moriishi, T., Yamana, K., Miyazaki, T., Toyosawa, S., and Komori, T. (2006) *Dev. Biol.* **296**, 48–61

34. Sakai, N., Wada, T., Furuichi, K., Shimizu, K., Kokubo, S., Hara, A., Yamahana, J., Okumura, T., Matsushima, K., Yokoyama, H., and Kaneko, S. (2006) *J. Leukoc. Biol.* **79**, 555–563

35. Furuichi, K., Gao, J. L., Horuk, R., Wada, T., Kaneko, S., and Murphy, P. M. (2008) *J. Immunol.* **181**, 8670–8676

36. Ma, B., Zhu, Z., Homer, R. J., Gerard, C., Strieter, R., and Elias, J. A. (2004) *J. Immunol.* **172**, 1872–1881

37. Shang, X., Qiu, B., Frait, K. A., Hu, J. S., Sonstein, J., Curtis, J. L., Lu, B., Gerard, C., and Chensue, S. W. (2000) *Am. J. Pathol.* **157**, 2055–2063

38. Anders, H. J., Frink, M., Linde, Y., Banas, B., Wörnle, M., Cohen, C. D., Vielhauer, V., Nelson, P. J., Gröne, H. J., and Schlöndorff, D. (2003) *J. Immunol.* **170**, 5658–5666

39. Coates, P. T., Colvin, B. L., Ranganathan, A., Duncan, F. J., Lan, Y. Y., Shufesky, W. J., Zahorchak, A. F., Morelli, A. E., and Thomson, A. W. (2004) *Kidney Int.* **66**, 1907–1917

40. Ishii, M., Egen, J. G., Klauschen, F., Meier-Schellersheim, M., Saeki, Y., Vacher, J., Proia, R. L., and Germain, R. N. (2009) *Nature* **458**, 524–528

41. Matsuo, K., and Irie, N. (2008) *Arch. Biochem. Biophys.* **473**, 201–209

42. Kitazawa, R., Mori, K., Yamaguchi, A., Kondo, T., and Kitazawa, S. (2008) *J. Cell Biochem.* **105**, 1289–1297

43. Murphy, P. M., Baggiolini, M., Charo, I. F., Hébert, C. A., Horuk, R., Matsushima, K., Miller, L. H., Oppenheim, J. J., and Power, C. A. (2000) *Pharmacol. Rev.* **52**, 145–176

44. Terashima, Y., Onai, N., Murai, M., Enomoto, M., Poonpiriya, V., Hamada, T., Motomura, K., Suwa, M., Ezaki, T., Haga, T., Kanegasaki, S., and Matsushima, K. (2005) *Nat. Immunol.* **6**, 827–835

45. Sato, K., Suematsu, A., Okamoto, K., Yamaguchi, A., Morishita, Y., Kadono, Y., Tanaka, S., Kodama, T., Akira, S., Iwakura, Y., Cua, D. J., and Takayanagi, H. (2006) *J. Exp. Med.* **203**, 2673–2682

46. Votta, B. J., White, J. R., Dodds, R. A., James, I. E., Connor, J. R., Lee-Rykaczewski, E., Eichman, C. F., Kumar, S., Lark, M. W., and Gowen, M. (2000) *J. Cell Physiol.* **183**, 196–207

47. Rioja, I., Hughes, F. J., Sharp, C. H., Warnock, L. C., Montgomery, D. S., Akil, M., Wilson, A. G., Binks, M. H., and Dickson, M. C. (2008) *Arthritis Rheum* **58**, 2257–2267

☑ Research article

Maf promotes osteoblast differentiation in mice by mediating the age-related switch in mesenchymal cell differentiation

Keizo Nishikawa,[1,2] Tomoki Nakashima,[1,2,3] Shu Takeda,[4] Masashi Isogai,[5] Michito Hamada,[5] Ayako Kimura,[4] Tatsuhiko Kodama,[6] Akira Yamaguchi,[7] Michael J. Owen,[8] Satoru Takahashi,[5] and Hiroshi Takayanagi[1,2,3]

[1]Department of Cell Signaling, Graduate School of Medical and Dental Sciences, Tokyo Medical and Dental University, Tokyo, Japan. [2]Global Center of Excellence Program, International Research Center for Molecular Science in Tooth and Bone Diseases, and [3]Japan Science and Technology Agency, ERATO, Takayanagi Osteonetwork Project, Tokyo, Japan. [4]Department of Orthopaedic Surgery, Graduate School of Medical and Dental Sciences, Tokyo Medical and Dental University, Tokyo, Japan. [5]Institute of Basic Medical Sciences and Laboratory Animal Resource Center, University of Tsukuba, Tsukuba, Japan. [6]Department of Molecular Biology and Medicine, Research Center for Advanced Science and Technology, University of Tokyo, Tokyo, Japan. [7]Department of Oral Pathology, Graduate School of Medical and Dental Sciences, Tokyo Medical and Dental University, Tokyo, Japan. [8]GlaxoSmithKline, Stevenage, United Kingdom.

Aging leads to the disruption of the homeostatic balance of multiple biological systems. In bone marrow multipotent mesenchymal cells undergo differentiation into various anchorage-dependent cell types, including osteoblasts and adipocytes. With age as well as with treatment of antidiabetic drugs such as thiazolidinediones, mesenchymal cells favor differentiation into adipocytes, resulting in an increased number of adipocytes and a decreased number of osteoblasts, causing osteoporosis. The mechanism behind this differentiation switch is unknown. Here we show an age-related decrease in the expression of *Maf* in mouse mesenchymal cells, which regulated mesenchymal cell bifurcation into osteoblasts and adipocytes by cooperating with the osteogenic transcription factor Runx2 and inhibiting the expression of the adipogenic transcription factor *Pparg*. The crucial role of Maf in both osteogenesis and adipogenesis was underscored by in vivo observations of delayed bone formation in perinatal *Maf*^{−/−} mice and an accelerated formation of fatty marrow associated with bone loss in aged *Maf*^{+/−} mice. This study identifies a transcriptional mechanism for an age-related switch in cell fate determination and may provide a molecular basis for novel therapeutic strategies against age-related bone diseases.

Introduction

A progressive and irreversible accumulation of DNA damage, which is triggered by telomere shortening and various stressors such as oxidative stress, contributes to cellular senescence and organismal aging (1, 2), but how aging is related to the disruption of the homeostatic balance of cell differentiation from a common progenitor is not well understood. Bone marrow contains multipotent mesenchymal progenitor cells, which differentiate into various anchorage-dependent cell types, including adipocytes and osteoblasts (3, 4). With age, mesenchymal cells in the bone marrow become inclined to undergo differentiation into adipocytes rather than osteoblasts (5–7), resulting in an increased number of adipocytes and a decreased number of osteoblasts, causing osteoporosis. Adipocytes are also known to directly inhibit functions of other cells in the bone marrow, including hematopoietic stem cells and osteoblasts (8–11). Since an increase in marrow fat along with bone loss is observed in diabetic patients treated with thiazolidinediones (TZDs) (12), understanding the mechanism of this differentiation switch has substantial relevance to both the management of age-related osteoporosis and secondary osteoporosis after such drug treatment. However, the change in mesenchymal cell differentiation cannot be adequately explained by cellular

senescence or the cell cycle arrest caused by DNA damage. While estrogen deficiency causes postmenopausal osteoporosis (6, 13), it has been suggested that the downregulation of cytokines and hormones, such as IGF1, TGFB1, IL-11, and growth hormone, is correlated with age-related bone loss (6, 14, 15). However, a cell-intrinsic mechanism that regulates the age-related switch in mesenchymal cell differentiation remains to be elucidated. Here we report an age-related decrease in the expression of *Maf* in mesenchymal cells and present evidence that Maf regulates mesenchymal cell bifurcation into osteoblasts and adipocytes. This study establishes the crucial role of the Maf-mediated transcriptional program in the physiological and age-related regulation of mesenchymal cell lineage, which may facilitate the development of new therapeutic strategies against bone and metabolic diseases.

Results

A genome-wide screening of transcription factors involved in the age-related decrease in bone formation. To identify the transcription factors involved in age-related bone loss, we performed a genome-wide screening of mRNAs expressed in cells derived from mouse calvaria during osteoblastogenesis. Among 1,470 transcription factors, we identified 163 genes related to osteogenic function; the identifying characteristic of these factors was that their expression was increased by more than 4-fold during osteoblastogenesis (Figure 1A and Supplemental Table 1, A and B; supplemental material
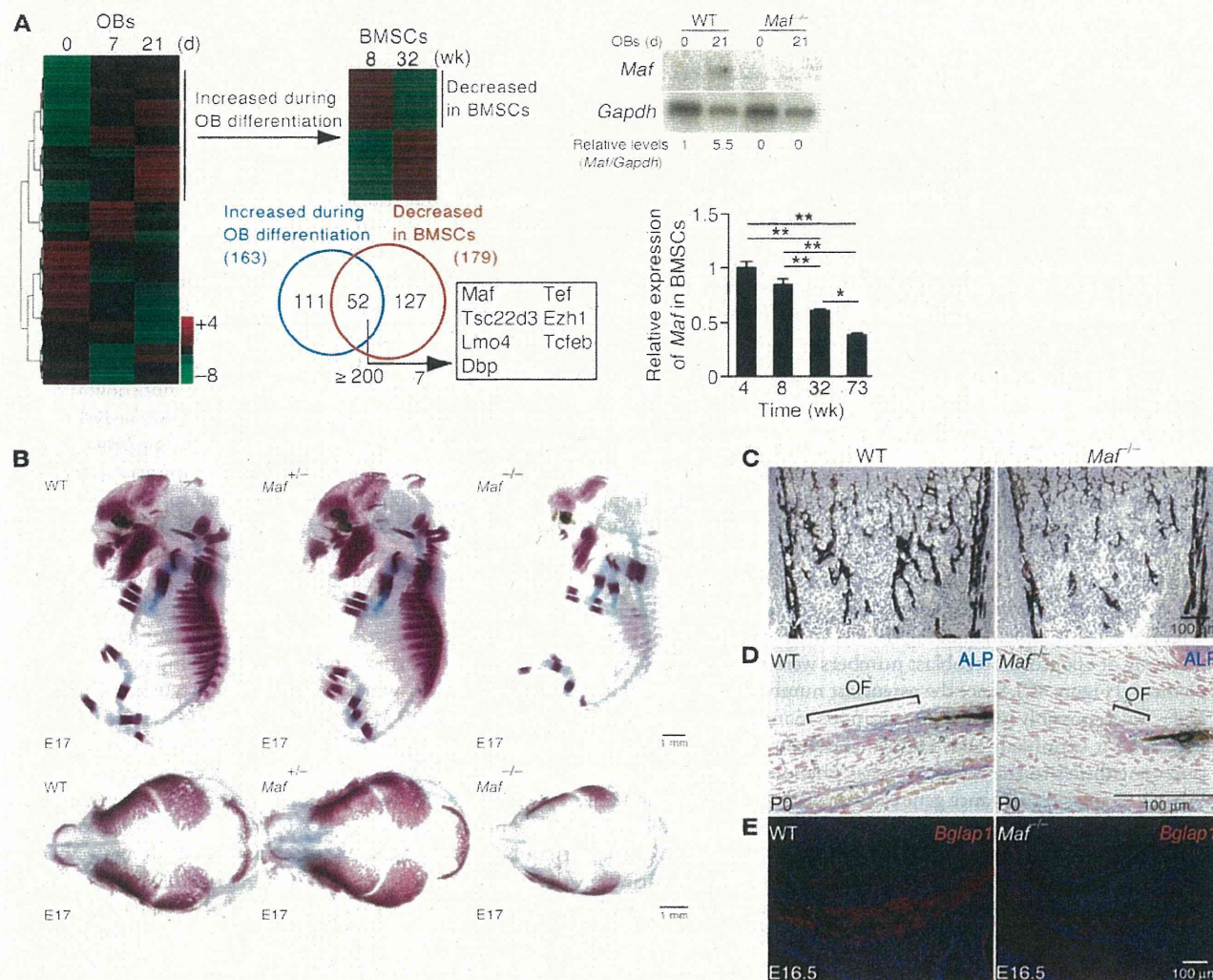
Figure 1
Impaired bone formation in *Maf⁻/⁻* mice. (**A**) A genome-wide screening of transcription factor mRNAs during in vitro differentiation of osteoblasts (OBs) and a comparison of their expression between 8- and 32-week-old BMSCs. The increase in *Maf* expression during osteoblastogenesis was confirmed in calvarial osteoblasts (RNA blot analysis, right top). *Maf* expression was markedly lower in BMSCs derived from the aged mice (real-time RT-PCR analysis, right bottom). Screening results are summarized in the Venn diagram. *$P < 0.05$; **$P < 0.01$. (**B**) Alizarin red/alcian blue staining of E17 embryos (top). Top view of calvaria (bottom). Images in **B** are composites. (**C**) Histology (von Kossa staining) and micro-computed tomography analysis of WT and *Maf⁻/⁻* littermates at P0 (*n* = 3). Scale bar: 100 μm. (**D**) ALP and von Kossa staining of osteogenic fronts (OFs) in the calvaria of WT and *Maf⁻/⁻* littermates. Scale bar: 100 μm. (**E**) Expression of *Bglap1* in the calvaria of WT and *Maf⁻/⁻* mice (in situ hybridization). Scale bar: 100 μm.

available online with this article; doi:10.1172/JCI42528DS1). To identify age-related genes, we also comprehensively analyzed the mRNAs expressed by bone marrow stromal cells (BMSCs) derived from 8- and 32-week-old mice, which resulted in identifications of 179 genes, the expression of which was decreased in the aged mice by more than 2 fold (Supplemental Table 1C). Fifty-two genes met both criteria (Supplemental Table 1D), from which we selected 7 genes preferentially expressed in BMSCs (with an average difference greater than 200). Among these 7 genes, we identified *Maf* (also known as c-Maf) to be the most highly expressed in the BMSCs. We confirmed that the expression of *Maf* increased during osteoblastogenesis, using calvarial and BMSCs (Figure 1A, right top, and Supplemental Figure 1A), and decreased with age (Figure 1A, right bottom, and Supplemental Figure 1B). *Maf*, a

basic leucine zipper transcription factor, is known to be involved in the regulation of diverse developmental processes such as lens fiber elongation (16) and Th2 cell differentiation (17, 18). Although it has been documented that transcription factors such as ΔFosb, Taz, Esr1, Msx2, and Cebpβ regulate the bifurcation of osteoblast/adipocyte differentiation (7, 19, 20), the expression of ΔFosb was increased in aged BMSCs (Supplemental Figure 2) and the other 4 factors were not included in the 179 age-related genes (Supplemental Table 1C). These results suggest that Maf is one of the potential candidate genes underlying an age-related decrease in osteoblastogenesis.

The indispensable role of Maf in osteogenesis. Since *Maf⁻/⁻* mice usually die immediately after birth (16), we investigated the role of Maf in osteogenesis by analyzing the skeletal development of perinatal

Table 1

Skeletal development of perinatal $Maf^{-/-}$ mice

	WT	$Maf^{-/-}$
BV/TV (%)	29.51 ± 0.15	23.56 ± 0.32[A]
Tb.N (mm^{-1})	13.43 ± 0.26	11.81 ± 0.33[B]
Tb.Sp (μm)	51.86 ± 1.59	64.98 ± 1.46[A]
Tb.Th (μm)	22.47 ± 0.03	20.36 ± 0.63[B]

Microcomputed tomography analysis of WT and $Maf^{-/-}$ littermates at P0. BV/TV, bone volume/tissue volume, Tb.N, trabecular number, Tb.Sp, trabecular separation, and Tb.Th, trabecular thickness. [A]$P < 0.01$. [B]$P < 0.05$.

$Maf^{-/-}$ mice. Bone formation was severely impaired in both the long and calvarial bones in the embryos of $Maf^{-/-}$ mice (Figure 1B), and bone volume was decreased in newborn $Maf^{-/-}$ mice (Figure 1C, Table 1, and Supplemental Figure 3). The formation of alkaline phosphatase–positive (ALP-positive) cells on an osteogenic front was markedly impaired in the calvaria of newborn $Maf^{-/-}$ mice (Figure 1D). In situ hybridization analysis revealed the expression of osteoblast genes, such as $Bglap1$ (encoding osteocalcin), but not of $Runx2$ was much lower in the embryos of $Maf^{-/-}$ mice than WT mice (Figure 1E and Supplemental Figure 4, A and B), although the proliferating or apoptotic osteoblast numbers were not different (Supplemental Figure 4C). Since the osteoclast number was decreased in $Maf^{-/-}$ mice, possibly in a cell-autonomous manner (Supplemental Figure 5), it is unlikely that abnormal osteoclastic bone resorption contributes to the low bone mass phenotype in $Maf^{-/-}$ mice. When a neomycin-resistance gene cassette was inserted into the Maf locus, chondrocyte development was reported to be affected in the mutant mice, but the mice were not perinatally lethal (18). In the current study, in which the coding sequence of Maf was entirely replaced by the $LacZ$ cassette, the mice were perinatally lethal and exhibited more severe chondrocyte abnormalities (Supplemental Figure 6). It is difficult to rule out the possibility that a defect in chondrocytes contributes to a skeletal phenotype in long bone, but $Maf^{-/-}$ mice exhibited a defective bone formation in flat bones, like the calvaria (Figure 1B), which are not formed by endochondral bone formation, suggesting a role of Maf in osteoblasts. To analyze a cell-autonomous defect in osteoblasts further, osteoblast differentiation was evaluated in an in vitro culture system of osteoblast precursor cells derived from the calvaria of newborn $Maf^{-/-}$ mice. ALP activity and bone nodule formation were markedly suppressed in $Maf^{-/-}$ cells (Figure 2A), but neither the proliferation nor apoptosis was affected (Figure 2B). These results collectively indicate that a complete lack of Maf led to an osteopenic phenotype, due to impaired osteoblast differentiation and bone formation.

Maf regulates osteoblast differentiation in cooperation with Runx2. The expression of various osteoblast-specific genes, including $Bglap1$, was severely suppressed in $Maf^{-/-}$ cells (Figure 2, C and D), but $Runx2$, a well-known transcriptional regulator of $Bglap1$ (21, 22), was normally expressed in $Maf^{-/-}$ mice (Supplemental Figure 4B). It is notable that Maf expression was not decreased in $Runx2^{-/-}$ calvarial osteoblasts (Supplemental Figure 7). These results prompted us to investigate whether Maf directly regulates the $Bglap1$ promoter. As expected, 5 Maf recognition element–like (MARE-like) sequences were contained in the 1,050-base $Bglap1$ promoter region (Figure 2E). A reporter gene assay indicated that Maf activates the $Bglap1$ promoter mainly through a region containing 3 proximal MARE-like sequences (MARE1–MARE3), which was included in

the proximal DNase hypersensitive site (23) and partially overlapped with osteoblast-specific element 1 (OSE1) (22) (Figure 2F). ChIP experiments showed that Maf is recruited to the region containing MARE1–MARE3 in primary osteoblasts (Figure 2G), suggesting that Maf directly regulates the $Bglap1$ promoter.

To gain insight into the transcriptional partners of Maf, we analyzed the Maf transcriptional network using a systems biology approach, based on protein-protein interaction databases and our own GeneChip analysis. Fos, Jun, Atf4, Nfat, and Runx2 were included among the transcription factors predicted to interact with Maf (Supplemental Figure 8). The function of these candidate partners was examined in the Maf-mediated activation of the $Bglap1$ promoter, which was found to be exclusively enhanced by the addition of Runx2 (Figure 2H and data not shown). Consistent with this, the transcriptional activity of Maf on the $Bglap1$ promoter was markedly decreased in $Runx2^{-/-}$ cells (Supplemental Figure 9). Maf bound to Runx2 in an immunoprecipitation assay (Figure 3 and Supplemental Figure 10), and immunohistochemical analysis showed that Maf was colocalized with Runx2 in calvarial osteoblasts (Supplemental Figure 11). Thus, these results suggest that Maf controls osteoblast differentiation by regulating osteoblastic gene expression mainly in cooperation with Runx2.

Maf suppresses adipogenesis by the downregulation of Pparg. We further characterized the $Maf^{-/-}$ calvarial cells using gene set enrichment analysis (GSEA), which revealed adipocyte-related genes to be highly enriched in $Maf^{-/-}$ cells (Supplemental Figure 12). Indeed, GeneChip data showed that the expression of adipocyte genes was upregulated in $Maf^{-/-}$ calvarial cells, even under the conditions optimized for osteoblast differentiation (Figure 4A). $Maf^{-/-}$ cells differentiated into oil red O–positive adipocytes more efficiently than WT cells (Figure 4B). Real-time RT-PCR analysis confirmed the expression of $Pparg$, the key transcription factor for adipogenesis, as well as that of $Fabp4$, $Slc2a4$, Lpl, $Acc1$, and $Cd36$, downstream effectors of Pparγ (24–26), to be markedly elevated in $Maf^{-/-}$ cells (Figure 4C and Supplemental Figure 13). To further investigate the role of Maf in osteoblast and adipocyte differentiation, we ectopically expressed Maf in C3H10T1/2 cells, a stromal cell line with a capacity to differentiate into both osteoblasts and adipocytes, and found that the introduction of Maf resulted in a severe blockade of adipocyte differentiation and an enhancement of osteoblast differentiation (Figure 4D and Supplemental Figure 14). Similar results were obtained using another stromal cell line, ST2, and BMSCs (Supplemental Figure 15, A–C). In addition, short hairpin RNA-mediated knockdown of Maf in ST2 cells resulted in a blockade of osteoblast differentiation and an acceleration of adipocyte differentiation (Supplemental Figure 15, D and E). Similar results were obtained using BMSCs (Supplemental Figure 15F). These results suggest that Maf promotes osteoblast differentiation and inhibits adipocyte differentiation in a cell-autonomous manner.

To understand the mechanism underlying the Maf-mediated inhibition of $Pparg$ expression and adipogenesis, we examined the effect of Maf on the transcriptional activity of Cebp, the family members of which are involved in the regulation of $Pparg$ (27, 28). Overexpression of Maf clearly suppressed the activation of the $Pparg$ promoter by Cebpα and Cebpδ but not that by Cebpβ (Figure 4E and data not shown). Since the introduction of mutation(s) into MAREs in the $Pparg$ promoter did not affect the inhibitory effect of Maf on Cebpδ activity, it is unlikely that Maf inhibited the $Pparg$ promoter activity by directly binding to MAREs (Supplemental Figure 16, A and B). EMSA revealed that Maf did not affect the